Calhoun
Institutional Archive of the Naval Postgraduate School

Calhoun: The NPS Institutional Archive

DSpace Repository

Theses and Dissertations | 1. Thesis and Dissertation Collection, all items

1987

Microstructural characterization of the heat affected zone of HSLA-100 steel GMA-weldment.

Potkay, Gary P.; Challenger, Kenneth D.

http://hdl.handle.net/10945/22363

Downloaded from NPS Archive: Calhoun

http://www.nps.edu/library

Calhoun is the Naval Postgraduate School's public access digital repository for research materials and institutional publications created by the NPS community. Calhoun is named for Professor of Mathematics Guy K. Calhoun, NPS's first appointed -- and published -- scholarly author.

Dudley Knox Library / Naval Postgraduate School
411 Dyer Road / 1 University Circle
Monterey, California USA 93943

DUDLEY KNOX LIBRARY
GRADUATE SCHOOL
93943-5002

NAVAL POSTGRADUATE SCHOOL
Monterey, California

THESIS

MICROSTRUCTURAL CHARACTERIZATION OF THE HEAT AFFECTED ZONE OF HSLA-100 STEEL GMA-WELDMENT

by

Gary P. Potkay

December 1987

Thesis Advisor: Kenneth D. Challenger

Approved for public release; distribution is unlimited

T234362

REPORT DOCUMENTATION PAGE

REPORT SECURITY CLASSIFICATION UNCLASSIFIED	1b RESTRICTIVE MARKINGS
SECURITY CLASSIFICATION AUTHORITY	3 DISTRIBUTION / AVAILABILITY OF REPORT Approved for public release; distribution unlimited
DECLASSIFICATION / DOWNGRADING SCHEDULE	
ERFORMING ORGANIZATION REPORT NUMBER(S)	5. MONITORING ORGANIZATION REPORT NUMBER(S)
NAME OF PERFORMING ORGANIZATION laval Postgraduate School	6b OFFICE SYMBOL (If applicable) 69
7a. NAME OF MONITORING ORGANIZATION Naval Postgraduate School	
ADDRESS (City, State, and ZIP Code) lonterey, CA 93943-5000	7b. ADDRESS (City, State, and ZIP Code) Monterey, CA 93943-5000
NAME OF FUNDING / SPONSORING ORGANIZATION	8b. OFFICE SYMBOL (If applicable)
9. PROCUREMENT INSTRUMENT IDENTIFICATION NUMBER	
ADDRESS (City, State, and ZIP Code)	10 SOURCE OF FUNDING NUMBERS

PROGRAM ELEMENT NO.	PROJECT NO.	TASK NO.	WORK UNIT ACCESSION

TITLE (Include Security Classification)

ROSTRUCTURAL CHARACTERIZATION OF THE HEAT AFFECTED ZONE OF HSLA-100 STEEL GMA-WELDMENT

PERSONAL AUTHOR(S) Potkay, Gary P.

TYPE OF REPORT	13b. TIME COVERED	14. DATE OF REPORT (Year, Month, Day)	15. PAGE COUNT
aster's Thesis	FROM _____ TO _____	1987 December	86

SUPPLEMENTARY NOTATION

COSATI CODES			18. SUBJECT TERMS (Continue on reverse if necessary and identify by block number)
FIELD	GROUP	SUB-GROUP	HSLA-100, GMAW-S, Retained Austenite

ABSTRACT (Continue on reverse if necessary and identify by block number)

A high strength low alloy steel, HSLA-100, is under development by the U. S. Navy. The research presented in this thesis evaluated the effect of cooling rate on the heat affected zone (HAZ) of Gas Metal Arc Weldments (GMAW). The cooling rate at 540°C after gas metal arc welding was varied from 22°C/second to 42°C/second by using different plate thickness, different preheat and interpass temperatures as well as different heat inputs. Mechanical property data is reported elsewhere but summarized in this thesis.

All welds met required strength and toughness. However, for all but the fastest cooling rate, the tensile test transverse to the weld failed in the weld metal rather than in the base metal as would be expected with HY-100 steel. No

DISTRIBUTION / AVAILABILITY OF ABSTRACT	21. ABSTRACT SECURITY CLASSIFICATION	
☒ UNCLASSIFIED/UNLIMITED ☐ SAME AS RPT. ☐ DTIC USERS	UNCLASSIFIED	
. NAME OF RESPONSIBLE INDIVIDUAL enneth D. Challenger	22b. TELEPHONE (Include Area Code) 408-646-3036	22c. OFFICE SYMBOL 69Ch

FORM 1473, 84 MAR 83 APR edition may be used until exhausted. All other editions are obsolete.

SECURITY CLASSIFICATION OF THIS PAGE
UNCLASSIFIED

19. ABSTRACT (continued)

failures occurred in the HAZ which indicates that the strength of the HAZ is not a strength limiting factor.

The HAZ microstructure was characterized by optical metallography, scanning and transmission electron microscopy. These microstructures were correlated with microhardness and the mechanical properties. Microconstituents of the coarse grain HAZ for all the weldments were predominately a mixture of low carbon, higher bainite and martensite. The microstructure is characterized by parallel laths and regions of high dislocation density and considerable amounts of retained austenite. The microstructure of the HAZ adjacent to the base metal was in general, an overaged region of polygonal ferrite grains with coarse copper precipitates.

Transmission electron microscopic (TEM) examination of the HAZ revealed a second phase between the bainitic laths, especially in the coarse grained HAZ. Dark field TEM and electron diffraction studies confirmed that this second phase was retained austenite. This austenite would have formed at temperatures where substitutional solid diffusion could occur and thus, austenite stablizing elements (and impurity elements) probably have partitioned into the austenite. This would make the austenite very stable and thus explain the reported excellent resistance to hydrogen assisted cracking exhibited by the HAZ of these welds.

UNCLASSIFIED
SECURITY CLASSIFICATION OF THIS PAG

Approved for public release; distribution is unlimited

MICROSTRUCTURAL CHARACTERIZATION OF THE HEAT AFFECTED ZONE OF HSLA-100 STEEL GMA-WELDMENT

by

Gary P. Potkay
Lieutenant, United States Navy
B.S. Mechanical Technology, Purdue University, 1980

Submitted in partial fulfillment of the
requirements for the degree of

MASTER OF SCIENCE IN MECHANICAL ENGINEERING

from the

NAVAL POSTGRADUATE SCHOOL
December 1987

Thesis
D7485
c.1

ABSTRACT

A high strength low alloy steel, HSLA-100, is under development by the U. S. Navy. The research presented in this thesis evaluated the effect of cooling rate on the heat affected zone (HAZ) of Gas Metal Arc Weldments (GMAW). The cooling rate at 540°C after gas metal arc welding was varied from 22°C/second to 42°C/second by using different plate thickness, different preheat and interpass temperatures as well as different heat inputs. Mechanical property data is reported elsewhere but summarized in this thesis.

All welds met required strength and toughness. However, for all but the fastest cooling rate, the tensile test transverse to the weld failed in the weld metal rather than in the base metal as would be expected with HY-100 steel. No failures occurred in the HAZ which indicates that the strength of the HAZ is not a strength limiting factor.

The HAZ microstructure was characterized by optical metallography, scanning and transmission electron microscopy. These microstructures were correlated with microhardness and the mechanical properties. Microconstituents of the coarse grain HAZ for all the weldments were predominately a mixture of low carbon, higher bainite and martensite. The microstructure is characterized by parallel laths and regions of high dislocation density and considerable amounts of retained austenite. The microstructure of the HAZ adjacent to the base metal

was in general, an overaged region of polygonal ferrite grains with coarse copper precipitates.

Transmission electron microscopic (TEM) examination of the HAZ revealed a second phase between the bainitic laths, especially in the coarse grained HAZ. Dark field TEM and electron diffraction studies confirmed that this second phase was retained austenite. This austenite would have formed at temperatures where substitutional solid diffusion could occur and thus, austenite stablizing elements (and impurity elements) probably have partitioned into the austenite. This would make the austenite very stable and thus explain the reported excellent resistance to hydrogen assisted cracking exhibited by the HAZ of these welds.

TABLE OF CONTENTS

I. INTRODUCTION- 13

II. BACKGROUND- 14

A. DEVELOPMENT OF HSLA-100 STEEL - - - - - - - - - - - - - - 14

B. INFLUENCE OF ALLOYING ELEMENTS OF HSLA-100- - - - - - - - 15

C. INFLUENCE OF HEAT TREATMENT ON PROPERTIES OF HSLA-100 - 18

D. PREVIOUS STUDIES - 18

III. EXPERIMENTAL PROCEDURE - - - - - - - - - - - - - - - - - - - 20

A. MATERIAL - 20

B. SAMPLE PREPARATION - 20

C. MICROHARDNESS MEASUREMENTS - - - - - - - - - - - - - - - 21

D. OPTICAL MICROSCOPY - 22

E. SCANNING ELECTRON MICROSCOPY - - - - - - - - - - - - - - 22

F. TRANSMISSION ELECTRON MICROSCOPY - - - - - - - - - - - - 23

1. Wafering of Material Along the HAZ - - - - - - - - - - 23

2. Thin Foil Preparation - - - - - - - - - - - - - - - - - 23

3. Observation in the Transmission Electron Microscope 24

IV. RESULTS - 25

A. MECHANICAL PROPERTIES - - - - - - - - - - - - - - - - - - 25

B. MICROSTRUCTURAL CHARACTERIZATION - - - - - - - - - - - - 27

1. Base Metal - 27

2. Weld Metal - 28

3. HAZ Adjacent to Fusion Line - - - - - - - - - - - - - 28

4. HAZ Adjacent to Base Metal- - - - - - - - - - - - - - 30

V. DISCUSSION OF RESULTS - 32

A. MECHANICAL PROPERTIES - - - - - - - - - - - - - - - - - - 32

B. MICROSTRUCTURAL CHARACTERIZATION - - - - - - - - - - - - 34

VI. CONCLUSIONS - 38

VII. RECOMMENDATIONS - 39

APPENDIX OF TABLES AND FIGURES - - - - - - - - - - - - - - - - - 40

LIST OF REFERENCES- 81

BIBLIOGRAPHY - 84

INITIAL DISTRIBUTION LIST - 85

LIST OF TABLES

1. CHEMICAL COMPOSITION OF HSLA-100 STEEL BASE PLATE AND WELDING CONSUMABLES - - - - - - - - - - - - - - - 41

2. HEAT TREATMENT OF HSLA-100 6.35 mm (1/4 INCH) AND 19 mm (3/4 INCH) PRODUCTION PLATES - - - - - - - - - - - - 42

3. WELDING CONDITIONS FOR HSLA-100 GMAW-S FLAT POSITION WELDMENTS- 42

4. MECHANICAL PROPERTIES OF HSLA-100 BASE PLATE - - - - - - - - - 43

5. CHARPY V-NOTCH TEST RESULTS FOR 19 MM (3/4 INCH) AND 6.35 MM (1/4 INCH) THICK, GMAW-S, FLAT POSITION WELDMENTS - 44

6. TENSILE PROPERTIES OF 19 MM (3/4 INCH) AND 6.35 MM (1/4 INCH) THICK GMAW-S, FLAT POSITION WELDMENTS - - - - - - - 45

7. WIDTH OF HAZ AND AVERAGE GRAIN SIZE PARAMETERS - - - - - - - - 46

LIST OF FIGURES

1. The Fe-Cu Binary Phase Diagram - - - - - - - - - - - - - - - - - 47

2. Macrosample of W123 - 48

3. Macrosample of W125 - 48

4. Macrosample of W119 - 49

5. Macrosample of W130 - 50

6. Location of TEM Wafer Cuts for
   a. W119- 51
   b. W130- 51

7. Location of TEM Wafer Cuts for
   a. W123 - 52
   b. W125 - 52

8. Impact Energy vs Temperature - - - - - - - - - - - - - - - - - - 53

9. Microhardness Profile of W-130 - - - - - - - - - - - - - - - - - 54

10. Microhardness Profile of W-119 - - - - - - - - - - - - - - - - - 55

11. Microhardness Profile of W-125 - - - - - - - - - - - - - - - - - 56

12. Microhardness Profile of W-123- - - - - - - - - - - - - - - - - 57

13. Optical Micrograph of Typical Bainitic Structure of Base Metal
   a. 6.35 mm (1/4 inch) plate - - - - - - - - - - - - - - - - - - - 58
   b. 19 mm (3/4 inch) plate- - -- - - - - - - - - - - - - - - - - - 58

14. TEM Micrograph of 6.35 mm (1/4 inch) Base Metal - - - - - - - 59

15. TEM Micrograph of 19 mm (3/4 inch) Base Metal - - - - - - - - 59

16. TEM Micrograph of 6.35 mm (1/4 inch) Base Metal- - - - - - - - 60

17. Optical Micrograph of HAZ of W130- - - - - - - - - - - - - - - - 61

18. Optical Micrograph of HAZ of W119- - - - - - - - - - - - - - - - 62

19. Optical Micrographs of W130
   a. Fusion Zone- 63
   b. Fusion Line - 63

c. Coarse HAZ - 63
d. Coarse HAZ - 63
e. HAZ - 63
f. Base - 63

20. Optical Micrographs of W119
a. Fusion Zone - 64
b. Fusion Line - 64
c. Coarse HAZ - 64
d. Coarse HAZ - 64
e. HAZ- 64
f. Base - 64

21. Optical Micrographs of W125
a. Fusion Zone - 65
b. Fusion Line- 65
c. Coarse HAZ - 65
d. Coarse HAZ - 65
e. HAZ - 65
f. Base - 65

22. Optical Micrographs of W123- - - - - - - - - - - - - - - - - - 66
a. Fusion Zone - 66
b. Fusion Line- 66
c. Coarse HAZ - 66
d. Coarse HAZ- 66
e. HAZ- 66
f. Base - 66

23. SEM Micrograph of W119 - 67
a. Fusion Line - 67
b. HAZ Adjacent to Base Metal - - - - - - - - - - - - - - - - - 67

24. TEM Micrographs of Course Grain HAZ-W130 - - - - - - - - - - - 68
a. Lath Structure with High Dislocation Density - - - - - - - 68
b. Lath Structure with High Dislocation Density - - - - - - - 68

25. TEM Micrographs of Coarse Grain HAZ W130
a. Dark Field of Figure 22b Illustrating Interlath
Distribution of Retained Austenite - - - - - - - - - - - - 69
b. Selected Area Diffraction, (002)γ Reflection
Arrowed, Adjacent Reflection is (110)α - - - - - - - - - 69

26. TEM Micrograph of Coarse Grain HAZ W119
a. Bright Field - Lath Structure- - - - - - - - - - - - - - - 70
b. Dark Field - Taken with (002)γ Reflection- - - - - - - - 70

27. TEM Micrograph of Coarse Grain HAZ of W125
a. Bright Field - 71
b. Dark Field using γ Reflection- - - - - - - - - - - - - - 71

28. TEM Micrographs of Coarse Grained HAZ W125 with Retained Austenite
a. Bright Field - 72
b. Dark Field using γ Reflection- - - - - - - - - - - - - - - - 72

29. TEM Micrographs of Coarse Grain HAZ of W123
a. Bright Field - 73
b. Dark Field Showing Micro-twins - - - - - - - - - - - - - - - 73

30. TEM Micrographs of W130
a. Bright Field - 74
B. Dark Field - 74

31. TEM Micrograph of W119
a. Bright Field - Coarse Copper Precipitates- - - - - - - - - 75
b. Dark Field - Coarse Copper Precipitates - - - - - - - - - - 75

32. TEM Micrograph of Retained Austenite Particles in W119
a. Dark Field - 76
b. Dark Field - 76

33. TEM Micrographs of W125
a. Bright Field - 77
b. Dark Field using an ϵ-copper Reflection- - - - - - - - - - 77

34. TEM Micrographs of W125
a. Bright Field - 78
b. Dark Field using an ϵ-copper Reflection- - - - - - - - - - 78

35. TEM Micrographs of W123
a. Bright Field - 79
b. Dark Field using an ϵ-copper Reflection- - - - - - - - - - 79

36. TEM Micrographs of W123 Polyganized Ferrite
Grains with Microtwins
a. Bright Field- 80
b. Dark Field - 80

ACKNOWLEDGMENTS

I wish to express my appreciation to my thesis advisor, Dr. Kenneth D. Challenger, for his patience and guidance with this work. A special note of thanks to Dr. J. Mauro Losz for the excellent transmission electron microscopy and for his invaluable assistance during the TEM and micrographic interpretation phases of this work. I would also like to thank Mr. Tom Kellog for all the laboratory support received while working in the Material Science area.

I would like to express my appreciation to Mr. R. J. Wong and the David Taylor Naval Ship Research and Development Center for providing the materials and requisite background information as well as being available for any questions which arose during the course of this research.

Finally, to my wife, Barbara, who has been a source of inspiration and encouragement throughout, I dedicate this work.

I. INTRODUCTION

The materials used in the construction of naval vessels are governed not only by mechanical properties but, just as importantly, by cost. The Naval Sea System Commands (NAVSEA) Material Fabrication Improvement goals for fiscal years 1983 through 1990 include the concepts of improved materials and welding processes to help minimize production costs. [Ref. 1] Through the use of high-strength low-alloy (HSLA) steels, the U. S. Navy hopes to obtain a high strength steel with excellent weldability and reduced fabrication costs.

In particular, they are seeking to develop a low carbon, copper precipitation strengthened steel in the 758 MPa (110 ksi) yield strength range which can be joined without costly preheat requirements. [Ref. 2]

As part of the certification process of HSLA-100, both the mechanical properties and microstructures of the various joining methods must be measured and analyzed. This research deals specifically with the Gas Metal Arc Welding process and the effects of varying cooling rates on the microstructure of the HAZ.

II. BACKGROUND

A. DEVELOPMENT OF HSLA-100 STEELS

The U. S. Navy is currently developing a steel with a yield strength of 689 MPa (100 ksi), good fracture toughness and resistance to both stress corrosion cracking in sea water and hydrogen assisted cracking. Currently, HY-100 fulfills the strength, toughness and weldability requirements, but has serious drawbacks in terms of welding costs, primarily due to the need to preheat for welding in order to avoid hydrogen assisted cracking.

The U. S. Navy has qualified a low carbon, copper precipitation strengthened steel, HSLA-80 (MIL-5-24645) for ship construction. It has excellent weldability and toughness that allows welding of plate thicknesses of up to 19 mm without pre-heat but is only capable of a yield strength of 552-621 MPa (80-90 ksi). Therefore, the development of HSLA-100 for ship construction is being carried out by the AMAX Material Research Center (AMRC) under contract N00167-85-C-0066 to the David Taylor Naval Ship Research and Development Center (DTNSRDC). To minimize the time from development to certification for processing, the HSLA-100 is to be a modification of the already qualified HSLA-80. [Ref. 2]

The development of HSLA steels is an example of evolutionary based research. Once a material is developed an effort is made to refine its properties and to find the methods of production and fabrication which combine the retention of those properties with the lowest cost.

For a true HSLA steel, the cost is usually comparable to carbon steels vice that for alloyed steels. [Ref. 3] However, HSLA-100 is not truly a low-alloy steel (3.5% Ni, 1.6% Cu) and expected to cost about 10% more than HY-100.

HSLA steels provide high strength by microalloying and controlling the phase transformation of austenite to ferrite to eliminate the requirement for any tempering. [Ref. 4] Strengthening mechanisms also include precipitation strengthening, grain refinement, solid solution strengthening and mechanical processing. [Ref. 5]

HSLA-80 employs the same percentage of niobium (0.02% - 0.06%) as does HSLA-100 and therefore, no increase in strength is expected from grain refinement [Ref. 5] and the contribution of solid solution strengthening would be minor [Ref. 6] therefore, precipitation strengthening and phase transformation products are the means used to obtain the appreciable increase in yield strength.

B. INFLUENCE OF ALLOYING ELEMENTS ON HSLA-100

The specifications for the chemical composition of the HSLA-100 base plate, along with the actual composition of heat #56422-16, is provided in Table 1.

The very low carbon content, only 0.03%, improves the weldability and notch toughness of the steel. The higher the carbon content, the higher the Ductile-to-Brittle Transition (DBTT).

Copper precipitates can provide large increases in strength in ferrite. The solubility of copper is a function of temperature. As temperature decreases, so does solubility. This produces the

precipitation of FCC ϵ-copper from a supersaturated α-phase by aging. Coherent BCC clusters of copper form, grow and then, after the peak strength is achieved, transform to the ϵ-phase particles mentioned previously. [Ref. 7]. These gains in strength can be made while maintaining good weldability and toughness. [Ref. 8] As an added bonus, the increase in the copper content of HSLA steels can also provide improved corrosion resistence [Ref. 9].

Improvements in strength and toughness of both base metal and heat affected zones (HAZ) of welds are achieved through the addition of nickel [Ref. 10, 11]. This is an austenite stabilizer and thus increases the range of temperatures over which austenite is stable. Nickel also contributes to the prevention of the formation of low melting point copper rich phases which can cause with hot shortness in copper bearing steels. [Ref. 8]

Manganese appears to lower the transition temperature of low-carbon steels and increase hardenability [Ref. 10]. It aids in ferrite grain size refinement [Ref. 12] and acts as an austenite stabilizer. Recrystallization of austenite is accelerated by the addition of manganese, which increases solubility of NbC in α-Fe and reduces the supersaturation of Nb and thus the rate of precipitation of NbC from γ-Fe. [Ref. 12]. However, too great an addition of Mn can cause embrittlement [Ref. 10].

Niobium is instrumental in ferrite grain size refinement. It accomplishes this at very low concentrations by forming carbonitrides

which are present in the austenite during hot rolling. Retardation of recrystallization and grain growth of austenite occurs due to deformation and strain induced precipitation of carbonitrides. [Ref. 12, 13] Thus the material can be strengthened without an increase in ductile to brittle transition temperature (DBTT) [Ref. 4].

Molybdenum and chromium added to steels to increase hardenability and chromium also improves corrosion resistance. [Ref. 14] In addition, Molybdenum may increase the strengthening affect of copper in iron-copper alloys [Ref. 15].

Both silicon and aluminum combine with nitrogen to form nitrides. Notch toughness can be improved by the stabilization of grain size due to aluminum nitrides. [Ref. 10] Aluminum can be used for deoxidation and for grain size control.

Sulfur can have a detrimental effect on notch toughness. However, in concentrations of less than 0.04% there is little effect on notch toughness for semi-killed and Si-killed steels. [Ref. 10]

Phosphorus produces several negative effects in steels and must be kept to a minimum. Phosphorus will cause decreases in notch toughness, raises DBTT, decreases upper shelf energy, can increase susceptibility to embrittlement and can cause formation of nickle phosphides. [Ref. 10, 16]

Silicon is used for deoxidation of the steel to ensure a fully killed steel. [Ref. 10] Silicon can also contribute to the prevention of hot shortness in copper containing steels. [Ref. 8]

C. INFLUENCE OF HEAT TREATMENT ON PROPERTIES OF HSLA-100

The Binary Phase Diagram for iron-copper is presented in Figure 1. HSLA-100 contains 1.45 to 1.75% copper. The initial heat treatment of the 6.35 mm base metal involved austenitizing at 900°C (Point A) for 15 minutes, water quenching and then aging at 690°C (Point B) for 45 minutes followed by air cooling. Similarly, the 19 mm base metal was austenitized at 900°C, but for 45 minutes, then water quenched and aged at 635°C (not shown) for 60 minutes before being air cooled. The austenitizing causes ϵ-copper to go into solid solution in the austenite (γ). Quenching creates a copper supersaturated ferrite and the aging process promotes the precipitation of a secondary ϵ-copper phase within the primary ferrite (α) phase. Maximum strength occurs when the precipitates are about 2.4 nm in diameter [Ref. 4] and coherent with the ferrite.

D. PREVIOUS STUDIES

Burna [Ref. 17] reported that with regard to the microstructure of the HAZ in NICOP (HSLA-80, MIL-5-24645), it can be welded without preheating as Hydrogen Assisted Cracking (HAC) is not expected to be a problem in the HAZ.

Coldren and Cox [Ref. 18] determined that utilizing copper precipitation strengthening in a low carbon bainitic structure, with approximately 3.5% Ni for toughness and 0.025% Nb for austenite grain size control, produced the optimum combination of strength and toughness. They also found that the quenching rate from the

austenitizing temperature effects the extent of strengthening due to copper precipitation.

Miglin, et al, [Ref. 19] noted that in a quenched and tempered NICOP, the DBTT is lowered because the fine Nb(C,N) precipitates promoted a small grain size.

Goodman, et al, [Ref. 20] determined that by aging iron containing copper, coherent, copper-rich clusters would be formed in the ferrite and they would grow by bulk diffusion. These copper precipitates are body centered cubic (BCC) and have less copper content than the equilibrium ϵ-phase. The face-centered cubic (FCC) ϵ-phase forms clusters during overaging. The peak strength is reached in a Fe-1.4 copper alloy where the average diameter of the BCC precipitates is about 2.4 nm; at this size, the precipitates were found to contain about 50% copper.

III. EXPERIMENTAL PROCEDURE

A. MATERIAL

Four samples of GMAW-S welded HSLA-100 were provided by DTNSRDC for microstructural characterization of the heat effected zones. All four samples were from Heat # 56422-16 produced by Phoenix Steel Corp under subcontract to AMRC. Two samples, W-123 and W-125, (Figs. 2 and 3) were from 6.35mm (1/4 inch) thick plate and two samples W-119 and W-130 (Figs. 4 and 5) were from 19 mm (3/4 inch) thick plate. The heat treatments for both the 6.35 mm and 19 mm plates are given in Table 2. The weld parameters were varied in order to create the four different cooling rates shown in Table 3. Weld current and voltage were constant for all four samples but the plate thickness, interpass temperature, travel speed and heat input were varied to create the different cooling rates. All welds were performed using consumables which met MIL-120S-1 (HY-100 filler metal) specifications (Table 1).

B. SAMPLE PREPARATION

The samples were cut perpendicular to the line of the weld into sections suitable for metallographic mounting. Samples for macroetching and optical microscopy were approximately 6 mm thick and were mounted using a fast cure acrylic. Samples to be used for TEM were cut to approximately 0.25 mm thick.

All four macrosamples were cold sanded and polished to a 6μm finish and then etched for approximately 10 minutes using a 2% Nital solution (2% nitric acid [HNO_3] and 98% ethanol [C_2H_5OH]) in order to reveal the weld passes and exact location of HAZ.

Microhardness and optical microscopy samples were prepared using standard metallographic techniques with a final polishing using 1 μm diamond compound. They were then etched for approximately 35 seconds in a 2% Nital solution.

C. MICROHARDNESS MEASUREMENTS

Samples were polished and etched with 2% Nital for approximately 35 seconds to highlight the fusion line and heat affected zone, which were the areas of primary interest. A line was scribed perpendicular to the fusion line, extending from the fusion zone through the HAZ and into the base metal as a guide from the hardness traverse. A Buehler microhardness tester, utilizing a 300 gram load with a diamond pyramid indentor and a 600X optical system was used to obtain the Vickers hardness measurements. The spacing between indents through the fusion line and coarse grain HAZ was 0.1 mm with larger spacing utilized in the fusion zone and well out into the HAZ and base metal.

At least two microhardness traverses were performed on each sample. For each sample, one microhardness traverse was taken through the last pass weld, a second traverse through a region reheated by a subsequent weld pass and, on the 19mm samples, a traverse was taken

near the bottom (first weld pass) of the weld. These traverses provided a way to compare the hardness of areas which were heat treated by subsequent passes and those which were not, as well as comparisons among individual samples.

D. OPTICAL MICROSCOPY

The hardness traverse of each sample was examined and compared with those of the other samples. In addition, optical micrographs, were taken at selected points along one microhardness traverse of each sample to determine the characteristics of the microstructure corresponding to a particular hardness measurement. The prior austenite grain size and bainite packet size were measured using the intercept method on samples etched in 2% Nital. The micrographs were taken at 500X and approximately 200 grains were counted for each sample. The lath widths were also measured using the intercept method on TEM micrographs at several different magnifications. In addition, montages of micrographs from both W-119 and W-130 were prepared in the region of the last weld pass, starting in the fusion zone through the coarse grain HAZ, at a magnification of 200X. A Zeiss ICM 405 Microscope was used for all examinations and the Zeiss MC 63 Photomicrographic Camera was used for all optical photomicroscopy.

E. SCANNING ELECTRON MICROSCOPE

A Cambridge Stereo Scan S4-10 scanning electron microscope (SEM) was employed. Micrographs of the microstructure in the coarse grain

heat affected zone at the fusion line and the HAZ/base metal interface were taken at a magnification of approximately 2300X.

F. TRANSMISSION ELECTRON MICROSCOPY

1. Wafering of Material Along the HAZ

Each sample was prepared by first grinding, polishing and etching a transverse face with 2% Nital for approximately 35 seconds. A scribe was then used to mark the fusion line and HAZ/Base Metal interface. An inital cut was made in the base metal region, parallel to the fusion line using an ISOMET Low Speed Wafering Machine. The sample was then remounted using this face as a reference point, and the first cut was made at the fusion line, with subsequent cuts passing through the HAZ into the base metal. The sample wafers were cut to a nominal thickness of approximately 0.25 mm. The wafer and remaining sample thicknesses were measured and recorded after each cut to maintain a map of wafer locations.

2. Thin Foil Preparation

Wafers from the weld metal adjacent to the fusion line, the coarse grain HAZ adjacent to the fusion line (Point A of Figures 6a and 6b and Figures 7 a and 7 b), the fine-grained HAZ adjacent to the base metal (Point B of Figures 6a and 6b and Figures 7a and 7b) and the base metal were then prepared for TEM. The wafers were first mechanically thinned to approximately 0.125 mm and then 3 mm diameter disks were punched from this wafer and thinned to approximately 0.09

mm using 600 grit paper. Final thinning was then accomplished using a Struers Tenupol and Streurs Polipower electropolishing apparatus. A Solution of 10% percloric acid ($HC1O_4$) and 90% acetic acid was used as the electrolyte and maintained at a temperature of +13°C. The power supply was maintained at 50-60 volts resulting in a current of 180-200 milliamps. The Tenupol's pump was set at a medium flow rate and a photo-cell circuit was set to terminate the electropolishing when the disk was perforated.

3. Observation in the Transmission Electron Microscope

The prepared disks were then examined using a JEM-120 CX MK II transmission electron microscope (TEM) using an accelerating voltage of 120 K_eV. The disks were observed at magnifications in the range of 10,000x to 67,000x.

IV. RESULTS

A. MECHANICAL PROPERTIES

With the exception of the microhardness readings, the data on the mechanical properties of the weldments presented was compiled by DTNSRDC. [Ref. 21] As shown in Table 4, the 6.35 mm and 19 mm thick HSLA-100 base plates had a 0.2% Offset Yield Strengths greater than 689 Mpa. It can be seen that the values for elongation and the reduction in area for the 6.35 mm base plate are very similar in both the transverse and longitudinal directions. Data is only available for the transverse direction for the 19 mm base plate.

Impact Energy vs Temperature for the 6.35 mm plate and for the 19 mm plate can be seen in Figure 8 and Table 4. The 6.35 mm plate utilized half size Charpy V-Notch (CVN) samples and therefore cannot be compared with the numerical values of the 19 mm plate. The plot for the 6.35 mm base plate material displays a linear increase in impact energy with temperature. In addition, when the available C_v impact energy for weldment W123 (Table 5) in the HAZ are plotted over this data, it can be seen that the HAZ material properties are similar to those of the base plate properties. Although there is only limited data available for the 19 mm plate, W119, it can again be seen from a comparison of the base metal and HAZ data, (Table 5) in Figure 8, that the HAZ properties are similar to the base metal (with the exception of the one very low result). Thus, welding has not markedly affected the DBTT for this plate.

The tensile properties for the GMAW-S flat position weldments, listed in Table 6, illustrate the uniformity in values of the 2% yield strength and ultimate tensile strength for each of the individual samples. Tests to assess joint efficiency were completed on transverse specimens and show failure in the weld metal for all except W130. This 19 mm weldment had the highest cooling rate of all the samples and failed, not in the HAZ, but in the base metal. This clearly shows that for cooling rates lower than 41.7°C/second. The weakest point lies in the weld metal rather than the HAZ or base metal.

The results of the microhardness traverses for each sample are plotted in Figures 9 through 11. Although there is a large amount of scatter in the data, each of the traverses tends to follow the same general trend. As the traverse starts in the fusion zone and moves toward the HAZ, a decrease in hardness is noted just prior to the fusion line. The hardness on the fusion line was in the range of 285 to 298 H_v. As the traverse passes across the fusion line, an immediate increase in hardness is noted. The values of the microhardness measurements of all four samples, have the least scatter in this region from the fusion line to approximately 1 mm into the HAZ.

The average of the maximum hardness readings obtained for all four samples is approximately 320 H_v. As the traverse continued past the 1 mm point in the HAZ, hardness starts to decrease slowly out to

approximately 2 to 3 mm. from the fusion line. In all cases, the coarse grain HAZ region is the hardest region in the entire weldment system.

B. MICROSTRUCTURAL CHARACTERIZATION

1. Base Metal

The microstructure of both the 6.35 mm and 19 mm base metal samples (Figs. 13a and 13b) is predominantely bainitic. The 6.35 mm plate displays a banded structure which is not apparent in the 19 mm plates.

TEM micrographs of the 6.35 mm and 19 mm base plates in Figures 14 and 15 respectively, show a lath-like morphology representative of bainite. In addition, coarse copper precipitates can be seen within the lathes and areas of high dislocation density are readily apparent.

The copper precipitates (Point A) and possibly retained austenite (Point B) can be more easily identified by comparing the light and dark field micrographs of the 6.35 mm base metal in Figures 16a and 16b. The higher aging temperature required to meet the yield strength properties (aim of 759-793 MPa) in the thin plate has resulted in relatively coarse copper precipitates. So coarse in fact that little or no strengthening can be expected from their presence.

The optical micrographs of Figures 17 and 18 are montages of the 19 mm weldments, W130 and W119. Region A is the fusion zone, where the HY-100 consumable is deposited. The arrows indicate the

fusion line and the solid metal adjacent to it (Region B). Region B will have been heat to just below the melting point and experiences the maximum cooling rate. This area is the coarse grain heat affected zone. Moving from the coarse grain HAZ toward the base metal one encounters a grain refined region followed by a region heated only into the intercritical region and finally an overaged region (softest) just adjacent to the unaffected base metal.

2. Weld Metal

Optical micrographs of the weld metal (plates a and b of Figures 19 - 21) immediately adjacent to the fusion line show a microstructure which is predominately acicular ferrite for all four samples. In some regions, the presence of side-plate ferrite was also noted. A detailed investigation of the fusion zone has been carried out by K. D. Mickelberry [Ref. 22].

3. HAZ Adjacent to Fusion Line

In the HAZ, a decrease in grain size with increased distance from the fusion line can be seen in the optical micrographs of plates c, d, and e of Figures 19 - 21. In addition, for the 19 mm samples, W130, which has the higher cooling rate, a much finer grain and bainite packet size and narrower HAZ width are present, as can be seen in Table 7, than for W119. Similarly, for the 6.35 mm samples, W125, which had the higher cooling rate, a finer grain and packet size than for W123 are apparent. Plate f of Figures 19 - 21 is the base metal.

The SEM revealed similar microstructural characteristics for all four weldments and representative samples at the fusion line and

the HAZ/Base interface of the microstructures are provided in Figures 23a and 23b. All of the weldments displayed very similar constituents in the coarse grain HAZ. The only real difference is grain size caused by differences in individual sample cooling rates.

The morphology of the low carbon bainite/low carbon martensite can be observed by TEM in the coarse grain HAZ of all four weldments (Figures 24, 26, 27 and 29). A microstructure of parallel laths can be observed in Figures 24a and 24b. Regions of high dislocation density and retained austenite can also be observed. Figure 25a is a dark field micrograph of Figure 24b and highlights the retained austenite between the laths. The diffraction pattern from the lath pattern of Figure 25a can be seen in Figure 25b. The arrow indicates the (002) γ diffracted beam selected to illuminate the previous dark field.

The coarse grained HAZ of the 19 mm weldments, W119, in Figure 26a and 26b, again has the parallel lath type morphology along with retained austenite and areas of high dislocation density.

The lath morphology can again be seen in the coarse HAZ of the 6.35 mm weldment, W125, as well as the retained austenite, in Figure 27a and 27b. Areas of retained austenite, with much larger particles (Figure 28a and 28b) than those previously shown, were found in some areas of the HAZ of all four weldments.

For W123, Figure 29a is the typical lath like morphology with areas of high dislocation density similar to areas seen previously, but the dark field view in Figure 29b shows the presence of

microtwins. The microtwins were observed in some localized regions in all the weldments but were not a major microstructural feature.

4. HAZ Adjacent to Base Metal

The transition from HAZ to base metal could generally be discerned macroscopically and microscopically by the use of a 2% nital etchant.

Figures 30a and 30b are TEM micrographs showing a region of ferrite with large copper precipitates for the W130 material. This region does not display the lath type morphology of the coarse grain HAZ. There are some small areas which have a lath type morphology and retained austenite, but in general, it is an overaged region of polygonized ferrite grains.

In the 19 mm weldment, W119, larger ferrite grains containing a coarse distribution of copper percipitates, can be seen in Figure 31a and 31b. In addition, large particles of retained austenite, can be seen in the dark field micrographs of Figures 32a and 32b.

A large ferrite grain in the 6.35 mm weldment, W125, containing coarse copper precipitates is illustrated in Figures 33a and 34a. Regions of coalescence of the copper precipitates can be observed in the dark field micrograph of Figures 33b and 34b.

The predominance of a polygonal rather than lath ferrite was observed in this region and Figures 35a and 35b once again show the ferrite grains with coarse copper precipitates. Figures 36a and 36b provide a clear view of not only the ferrite grains, but also, a

localized region of microtwins. Although not predominant, the microtwins were present in all the materials observed in this region.

The TEM in this region of the HAZ has revealed that the distribution of copper in the alloy is not homogeneous at this scale of examination. Some polygonal grains exhibit a large number of Cu-precipitation and others none, Figures 33-35.

V. DISCUSSION OF RESULTS

The variable of interest in this research is the cooling rate of each individual weldment. Table 3 presents the coding rates for each weldment. W130 (19 mm) has the highest cooling rate followed by W125, W123 and finally W119, which had the highest heat input and slowest cooling rate.

The different cooling rates were produced by varying the plate thicknesses, the pre-heat temperature and, in the case of W119, the travel speed and thus the heat input rate. The 6.35 mm samples differed only in pre-heat temperatures, while the 19 mm samples had two variables, the different pre-heats, as well as heat inputs.

A. MECHANICAL PROPERTIES

The results of the mechanical testing completed by DTNSRDC [Ref. 21] demonstrate that the HSLA-100 base metal plates exhibited satisfactory tensile strength (Table 6). In addition, all CVN tests produced acceptable values of impact energy for both the 6.35 mm and 19 mm thick base plates.

In the limited tensile test results provided on all four weldments (Table 6), no failures occurred in the HAZ of any of the samples. In three cases, W125, W123 and W119, failure occurred in the fusion zone, while failure in the weldment with the highest cooling rate, W130, occurred in the base metal.

While CVN data in the HAZ was available for only two of the weldments, W119 and W123 (half size CVN speciman), the impact energies were consistent with those determined for the base metal plates at corresponding temperatures (Figure 5 and Table 6).

Microhardness traverses completed during this work compare favorably with the microhardness profiles determined by Wong on this same material (Figure 2 of Reference 21). In general, the data agreed within approximately ± 25 H_v. Measurements in the weld metal were relatively constant with a slight decrease in hardness just prior to the fusion line, possibly due to the mixing of weld metal and base-metal. A sharp increase in hardness was noted as the fusion line was crossed into the HAZ.

For all four weldments, the region starting at the fusion line and extending approximately 1 mm into the coarse grain HAZ, had hardness measurements which most closely approached a common average hardness. This area also displayed the highest individual H_v values. The highest H_v value in the HAZ for the 6.35 mm and 19 mm weldments occurred in the samples with the highest cooling rates.

Hardness values began to decrease with distance from the fusion line into the HAZ. This corresponds to the decrease in grain size as shown in plates B, C, D and E of Figures 19 - 21. This change in observed grain size corresponds to the decrease in the peak temperature reached during welding from the fusion line into the coarse grain HAZ and finally to the base metal. The cause of the large amount of scatter in the data was not determined. It may possibly have been due to chemical inhomogenity.

B. MICROSTRUCTURAL CHARACTERIZATION

Both the 6.35 mm and 19 mm base metal plates display a predominantly bainitic structure. However, the 6.35 mm plate displays the banding characteristic of alloying element segregation which can occur during solidification and then becomes alligned and elongated during hot rolling.

The TEM micrographs of the 6.35 mm and 19 mm base metal in Figures 14 and 15 exhibit both a lath-type bainitic microstructure, and a more polygonized ferrite morphology which must be a result of a the aging process. The laths consist of parallel ferrite plates characteristic of upper bainite and contain areas of high dislocation density.

BCC clusters of copper initially precipitate with an approximate size of 0.8 nm and increasing in size with aging time. [Ref. 23] These precipitates transform to FCC at 1 to 2.4 nm and this size coincides with peak strength. A mixture of coherent and incoherent copper particles along with the Nb(C,N) precipitates are produced. As reported by Miglin, et al, the Nb(C,N) precipitates contribute to ferrite grain refinement, reducing DBTT and provide a precipitation hardening effect while the copper precipitates act as a major strength contributor. [Ref. 24]

In the past, the coarse grain HAZ has received the most attention due to its poor mechanical properties. The large prior austenite grain size and the dissolution of all Nb(C,N) increases the hardenabililty and, as a result, low temperature transformation products form. At heat inputs characteristic of GMAW processes, the

microstructure seems to be largely upper bainite. However, the welds can have regions of mixed bainite/martensite microstructures. The combination of large austenite grain size with limited numbers of nucleation sites gives rise to coarse structures. The bainite grows as packets of almost parallel laths with low angle (or occasionally as shown previously in Figure 29 twin related) boundaries.

Although controversy exists as to the precise mechanism of formation, the ferrite laths appear to form at least in part by a shear transformation mechanism. The rapid formation of packets of parallel laths is suggestive of a sympathetic nucleation effect. Alloying elements which are more soluble in austenite (N,C,Ni) and some impurities diffuse into the austenite ahead of the γ/α interface as the ferrite laths grow and a layer of alloy rich austenite is eventually entrapped between the laths. The austenite may be retained in the final structure, transformed to martensite, or, as is most often the case, transformed to layers or particles of cementite extending along the lath boundaries. The cementite particles may be widely spread, or in some cases almost non-existent (as in the present case) because of the low carbon content in the steel studied.

The laths in upper bainite have the identical variant of the Kurdjumov-Sachs relationship, therefore misorientation of the laths with respect to each other is slight. Again, this means the longitudinal boundaries are low angle boundaries [Ref. 25].

The presence of stable retained austenite between the laths may contribute to improved toughness and possibly resistance to hydrogen

assisted cooling. Interlath retained austenite in Fe/1Cr/1Mo/0.3C steel appeared to contribute to improved Charpy impact energies where compared to Fe/Mo/C steels [Ref. 26]

There has been considerable discussion into whether Nb(C,N) can precipitate in the coarse grain HAZ. Generally, Nb(C,N) precipitation does not occur in the coarse grain HAZ during GMAW of plates having thicknesses of about 15 mm because of the combination of fast cooling rate and low transformation temperature. Certainly Nb(C,N) precipitation cannot occur at the cooling rates typical of most welding processes. However, with the trend towards higher heat inputs, Nb(C,N) precipitation has become a concern.

In regions of the HAZ where A_{c3} is exceeded, but sufficient Nb(C,N) is present to restrict grain growth, the austenite grain size is small and equiaxed, as is typical of a normalized steel. The low Nb and C concentrations and fine grain size of the austenite matrix cause high transformation temperatures and the formation of polygonized ferrite. This higher transformation temperature also permits sufficient diffusion for Nb(C,N) to precipitate during or shortly after transformation to ferrite.

The Rosenthal equation could be utilized to develop a relationship between grain size in the HAZ and temperature. This would allow the calculation of the temperature distribution with respect to observed microstructure. [Ref. 27]

The HAZ immediately adjacent to the base metal never exceeds the A_{c1} temperature and so an $\alpha \rightarrow \gamma$ transformation did not occur. This

region is marked by precipitate growth (Figures 31b, 33b, 34b, and 35b) dislocation annihilation (Figures 231, 33a, 34a, and 35a) and aging. [Ref. 28]

The large FCC copper precipitates can be seen dispersed in a polygonized ferritic grain structure. In general, this region does not seem to display the lath-type morphology of the base metal. It undergoes overaging which would account for the decrease in dislocations and the larger ferrite grains containing coarse FCC copper precipitates. Large particles of stable retained austenite (Figure 30) can be found in this region.

Stress corrosion cracking can be a problem in quenched and tempered HSLA steels. The mechanism most probable for a 690 MPa HSLA steel would be cracking caused by hydrogen embrittlement. [Ref. 29] However, HSLA-100 steel, with retained austenite may have improved resistance to SCC. Ritchie, et al [Ref. 30] determined that in isothermally transformed AISI 300-M steel, containing 12% retained austenite, had increased resistance to SCC compared to the same steel quenched and tempered (no retained austenite) to the same strength level. This was determined to probably be due to a reduction in hydrogen diffusevity which is much lower in FCC austenite.

The retained austenite between the laths may provide a barrier to hydrogen diffusion ahead of a crack tip. A lower bainitic structure is also reported to have lower rates of hydrogen diffusion than martensite. [Ref. 30]

VI. CONCLUSIONS

1. The microstructure of the four weldments were similar when compared at equivalent distances from the fusion line.
2. Grain size was dependent on cooling rates, with higher cooling rates producing a smaller grain size.
3. A lath-type morphology is present in the base metal and coarse grained HAZs. TEM micrographs show what appears to be a low carbon upper bainite/low carbon martensite structure with stable inter-lath retained austenite.
4. No significant effect of cooling rate in the range of 20.4°C/second to 41.7°C/second on the mechanical properties or the microstructure of the HAZ was observed.

VII. RECOMMENDATIONS

The role of retained austenite on the properties of this alloy must be clarified. This is potentially the principal reason why these steels exhibit excellent weldability and resistance to HAC.

APPENDIX

OF

TABLES

AND

FIGURES

TABLE 1. CHEMICAL COMPOSITION OF HSLA-100 BASE PLATE AND WELDING CONSUMABLES. [Ref. 21]

Element	Base Plate Spec*	Base Plate Heat #56422-16**	Electrode Spec. MIL-120S-1	120S-1 Wire***
Carbon	0.06 max	0.03	0.10 max	0.07
Manganese	0.75-1.05	0.86	1.40-1.80	1.54
Silicon	0.40 max	0.25	0.25-0.60	0.36
Phosphorus	0.015 max	0.005	0.01 max	0.007
Sulfur	0.006 max	0.002	0.01 max	0.005
Nickel	3.35-3.65	3.47	2.00-2.80	2.28
Molybdenum	0.55-0.65	0.61	0.30-0.65	0.47
Chromium	0.45-0.75	0.57	0.60 max	0.29
Vanadium	--	--	0.03 max	<0.01
Aluminum	0.02-0.04	0.033	0.10 max	0.02
Titanium	--	--	0.10 max	<0.01
Copper	1.45-1.75	1.53	--	0.01
Niobium	0.02-0.06	0.029	--	--
Zirconium	--	--	0.10 max	0.01
Nitrogen	0.015 max	0.014	--	--
Oxygen	--	--	--	--
Boron	--	--	--	--

*Purchase specification - contract N00167-85-R-0066
**Data provided by AMAX
***Analysis provided by the producer, Linde
+Analysis provided by the producer, Alloy Rods

TABLE 2. HEAT TREATMENT OF HSLA-100 6.35 mm (1/4 IN) AND 19 mm (3/4 IN) THICK PRODUCTION PLATE. [Ref. 31]

Identification	Austenitized		Quench	Aged		Cooling
	Temp (°C)	Time (min)		Temp (°C)	Time (min)	
GJY 6.35 mm (1/4 inch) thick	898.9	45	Water	690.6	45	Air
GJX 19 mm (3/4 inch) thick	898.9	45	Water	635.0	60	Air

TABLE 3. WELDING CONDITIONS FOR HSLA-100 GMAW-S FLAT POSITION WELDMENTS. [Ref. 21]

Identification	Plate Thickness (mm)	Preheat/ Interpass Temp (°C)	Voltage (V)	Current (amp)	Travel Speed (mm/sec)	Heat Input (kJ/mm)	Cooling Rate °C/sec
W130	19	51.6	26	260	5.72	1.18	41.7
W125	6.35	23.8	26	260	5.72	1.18	33.4
W123	6.35	51.6	26	260	5.72	1.18	21.6
W119	19	93.3	26	260	3.81	1.77	20.4

TABLE 4. MECHANICAL PROPERTIES OF HSLA-100 BASE PLATE. [Ref. 21]

Identification	Location	Orientation (L/T)	YS 0.2% Offset (MPa)	UTS (MPa)	EL (%)	RA (%)
GJY - 6.35 mm (1/4 inch) thick	Top	L	876	883	22	50
	Top	T	889	896	23	53
	Bottom	L	786	834	26	62
	Bottom	T	855	862	22	57
GJX - 19 mm (3/4 inch) thick	Top	T	765	924	22	75

Identification	Test Temperature (°C)	Impact Energy (J)
GJY 6.35 mm (1/4 inch) thick	99	81, 80, 79
	21	81, 79, 77
	- 1.11	79, 80, 81
	-17.80	80, 69, 69
	-40.00	75, 76, 71
	-62.20	68, 72, 66
	-84.40	71, 69, 60
GJX 19 mm (3/4 inch) thick	-17.80	233, 222, 228
	-84.40	152, 171, 161

Notes:
1. All values from 6.35 mm (1/4 inch) thick plates are from subsize specimens.
2. All specimens notched in T-L orientation

TABLE 5. CHARPY V-NOTCH TEST RESULT FOR 19 mm (3/4-INCH) AND 6.35 mm (1/4-INCH)THICK GMAW-S, FLAT POSITION WELDMENTS. [Ref. 21]

Identification	Nominal Heat Input (kJ/mm)	Plate Thickness Cooling Rate (°C)	Notch[1] Location	Test Temperature (°C)	Impact Energy (J)	% Shear
W130	1.18	41.7	Weld	-51	81	60
			Weld	-51	88	65
			Weld	-51	66	60
			Weld	-18	106	85
			Weld	-18	87	50
			Weld	-18	103	85
W125[2]	1.18	33.4	Weld	-51	33	not
			Weld	-51	37	recorded
			Weld	-51	39	for half
			Weld	-18	41	size CVN
			Weld	-18	41	
			Weld	-18	52	
W123[2]	1.18	21.6	Weld	-51	62	not
			Weld	-51	47	recorded
			Weld	-51	58	for half
			Weld	-18	43	size CVN
			Weld	-18	52	
			Weld	-18	43	
			HAZ	-51	63	
			HAZ	-51	68	
			HAZ	-51	76	
W119	1.65	20.4	Weld	-51	102	45
			Weld	-51	37	30
			Weld	-51	69	45
			Weld	-18	79	60
			Weld	-18	87	65
			Weld	-18	107	70
			HAZ	-51	121	85
			HAZ	-51	195	98
			HAZ	-51	197	100
Weld Metal Minimum Requirements				-51	47	
				-18	81	

1. All specimens notched in T-L orientation
2. Half size CVN specimen results are reported for the 6.35 mm (1/4-inch) weldments.

TABLE 6. TENSILE PROPERTIES OF 19 mm (3/4 INCH) and 6.35 mm (1/4 INCH) THICK GMAW-S, Flat Position Weldments. [Ref. 21]

Identification	Nominal Heat Input (kJ/mm)	Cooling Rate (°C/sec)	Orientation (L/T)	YS 0.2% Offset (MPa)	UTS (MPa)	EL (%)	RA (%)
W130	1.18	41.7	L	848	896	22	58
			L	862	903	16	66
			T	*	862	base	plate**
			T	*	827	base	plate**
W125	1.18	33.4	L	731	979	26	60
			L	717	938	28	68
			T	*	896	weld	metal+
			T	*	896	weld	metal+
W123	1.18	21.6	L	779	876	26	72
			L	717	841	29	70
			T	*	848	weld	metal+
			T	*	848	weld	metal+
W119	1.77	20.4	L	793	862	27	48
			L	827	889	29	66
			T	*	876	weld	metal+
			T	*	876	weld	metal+
Weld Metal Minimum Requirements			L	703 786	info	14	info

* Transverse tensile specimens are used to assess joint efficiency. The principle information derived is the ultimate tensile strength of the composite (weld, HAZ, and base plate) specimens.

** Fracture occurred in the base plate of the traverse specimen.

\+ Hydrogen damage observed on the fracture surface.

TABLE 7. WIDTH OF HAZ AND AVERAGE GRAIN PARAMETERS

Sample	HAZ Thickness (μm)	Prior Austenite Grain Size (μm)	Packet Size (μm)	Average Lath Width (μm)	Cooling Rate* °C
W130	2.6	40	20	0.206	41.7
W125	2.5	43	28	0.286	33.4
W123	3.2	53	30	0.334	21.6
W119	3.65	101	36	0.327	20.4

*Ref. 21

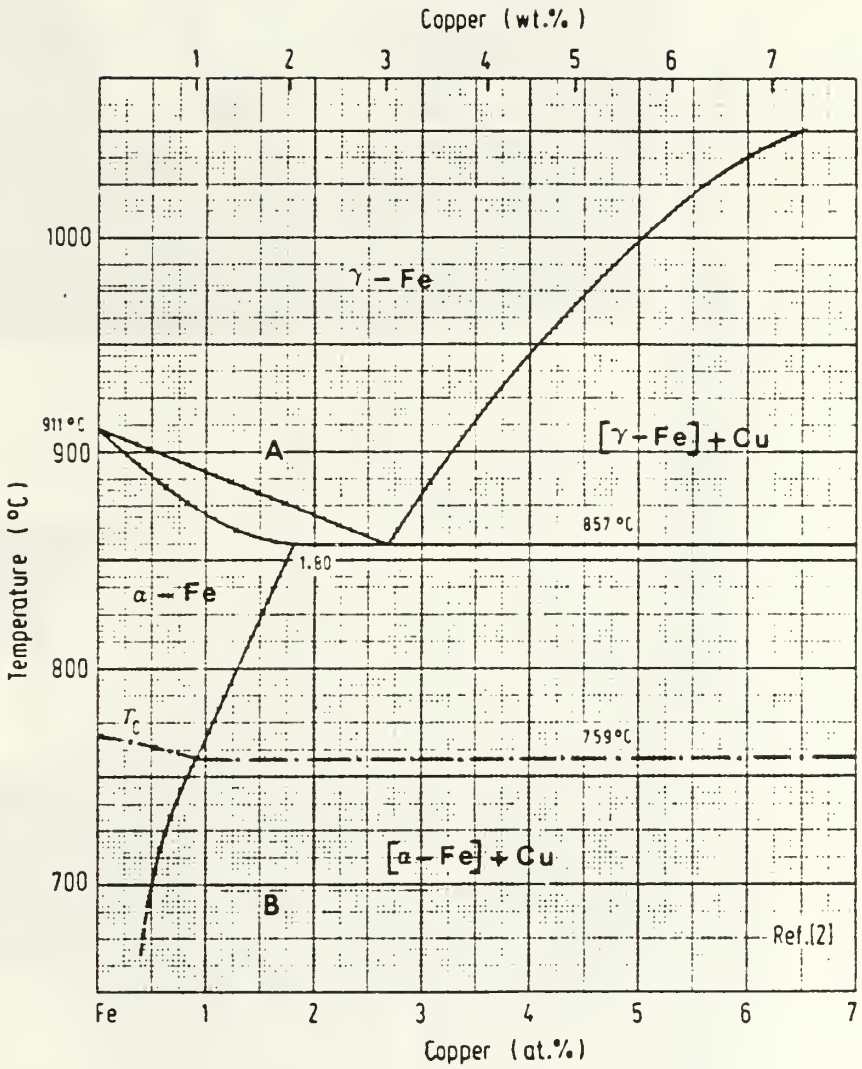

Figure 1. The Fe-Cu Binary Phase Diagram [Ref. 32]

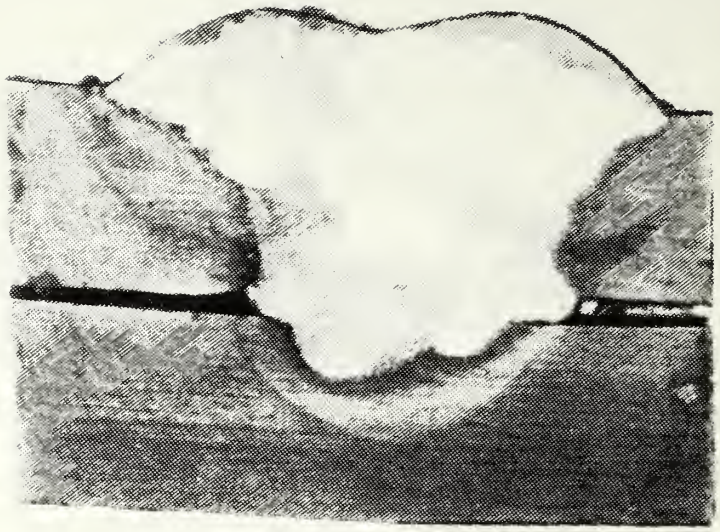

Figure 2. Macrosample of W123

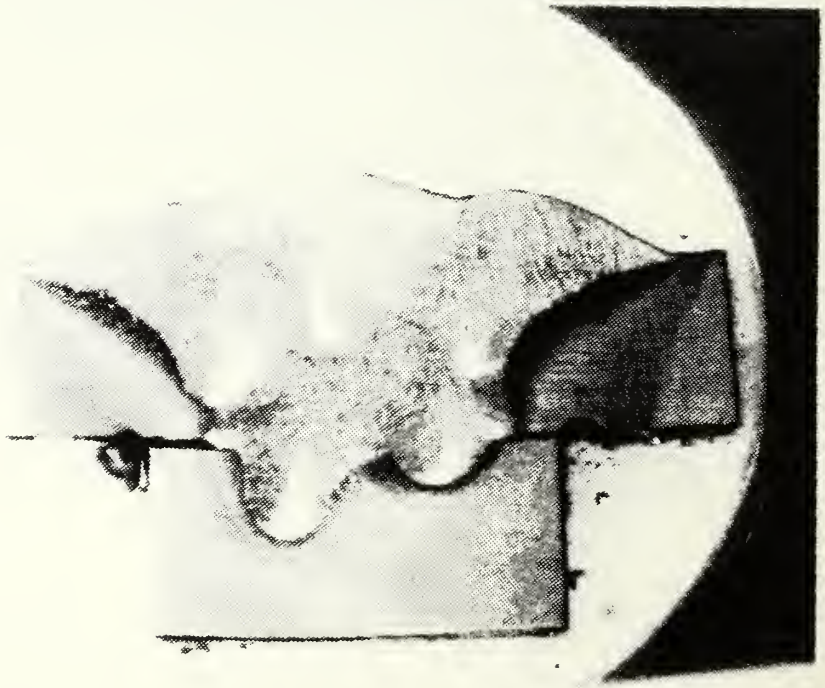

Figure 3. Macrosample of W125

Figure 4. Macrosample of W119

Figure 5. Macrosample of W130

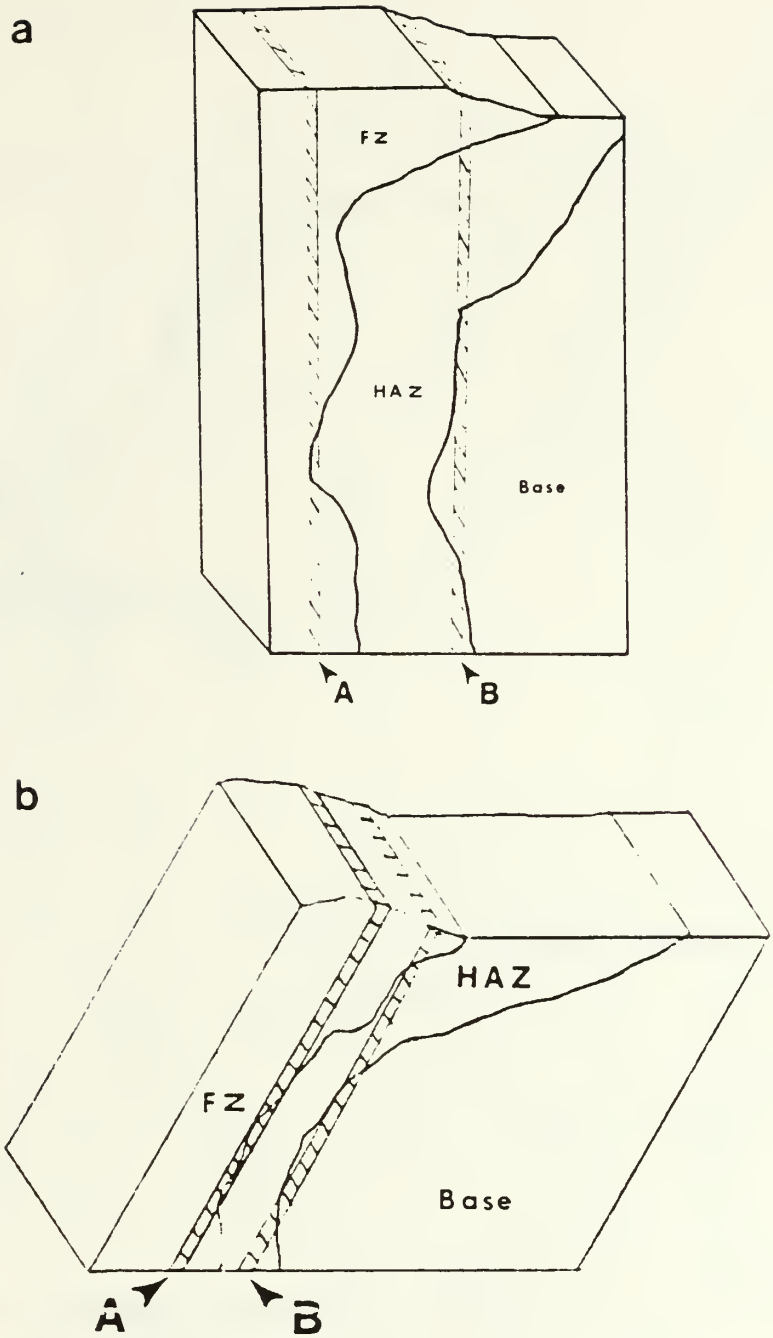

Figure 6. Location of TEM Wafer Cuts for
a. W119 b. W130

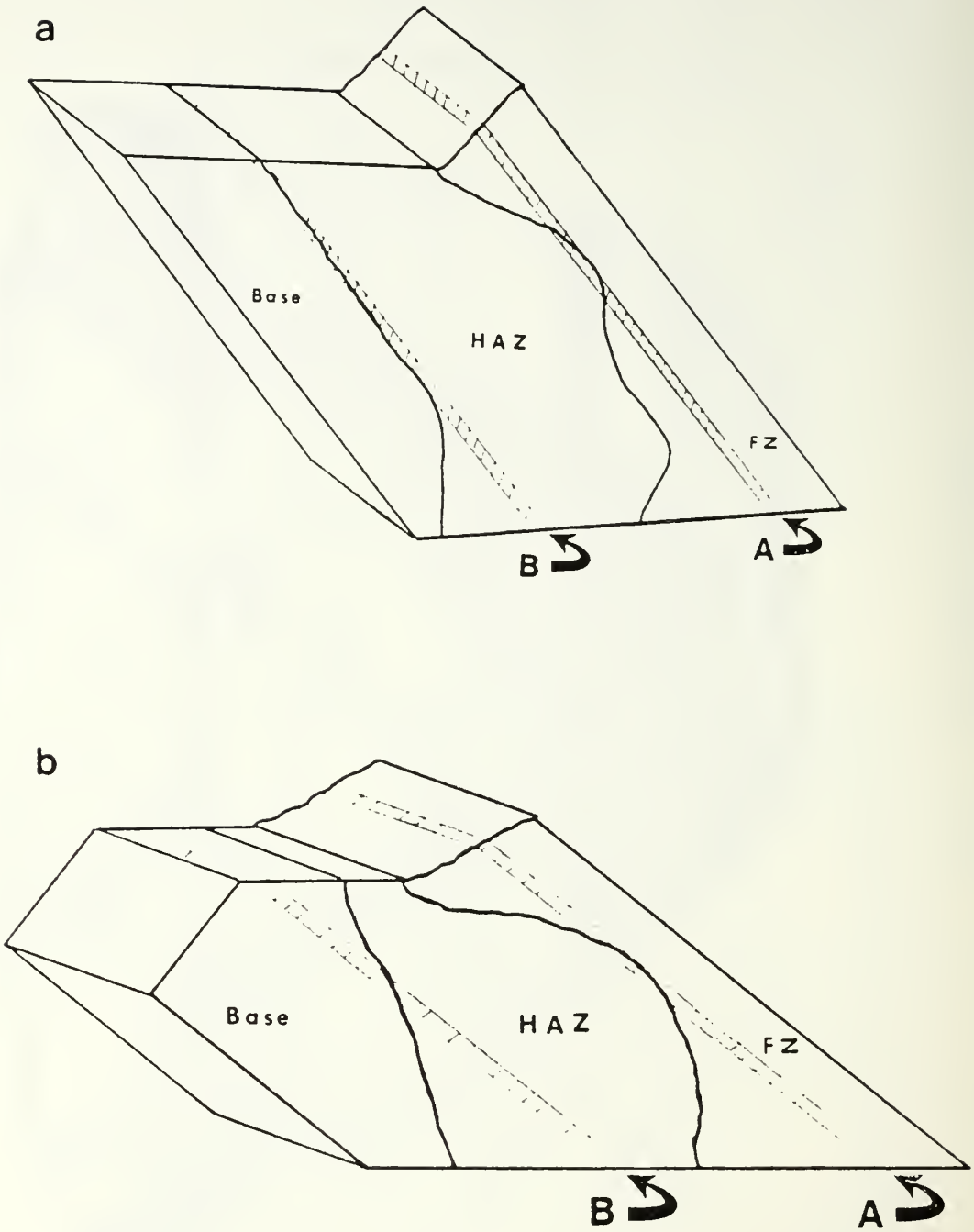

Figure 7. Location of TEM Wafer Cuts for
a. W123 b. W125

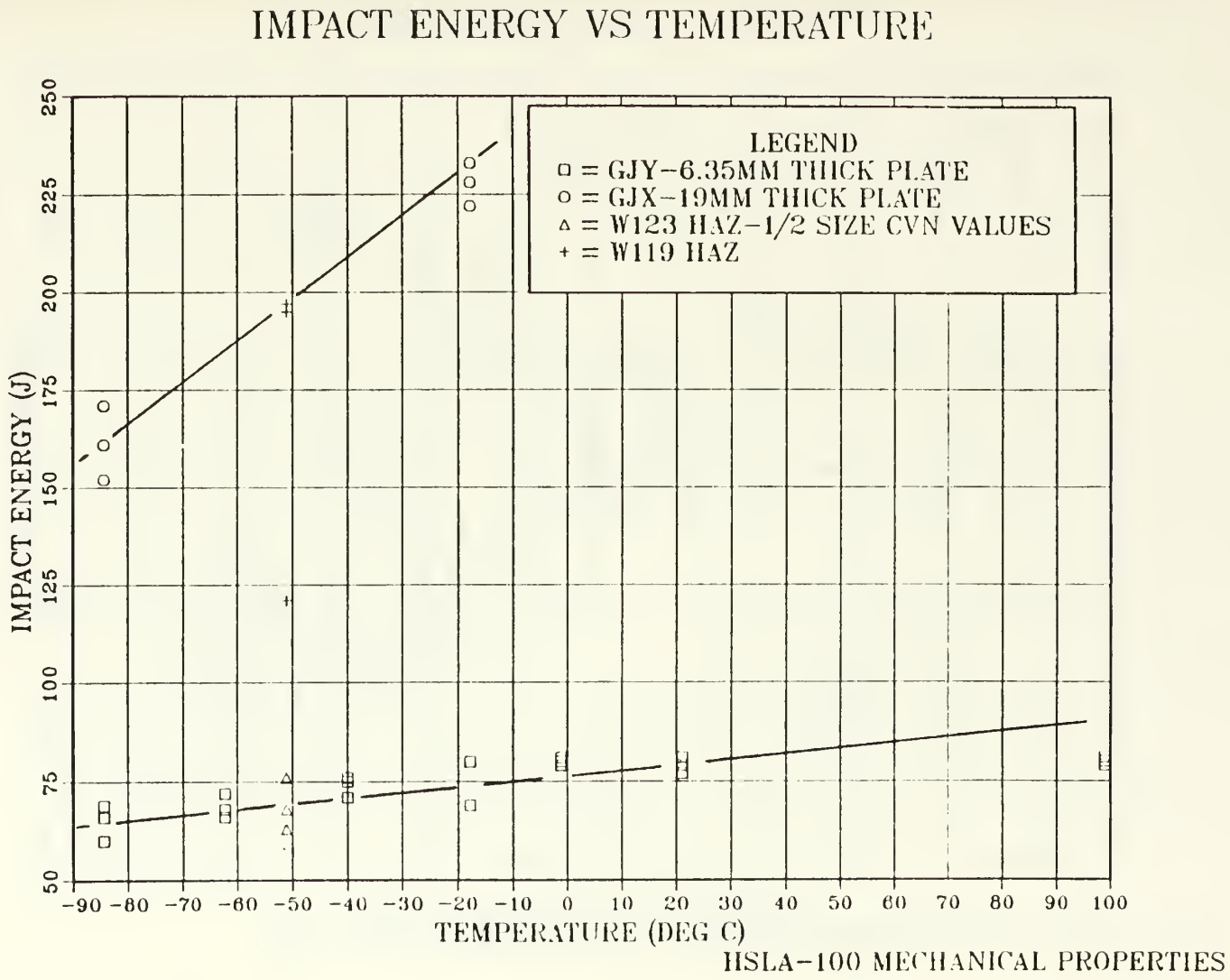

Figure 8. Impact Energy vs Temperature

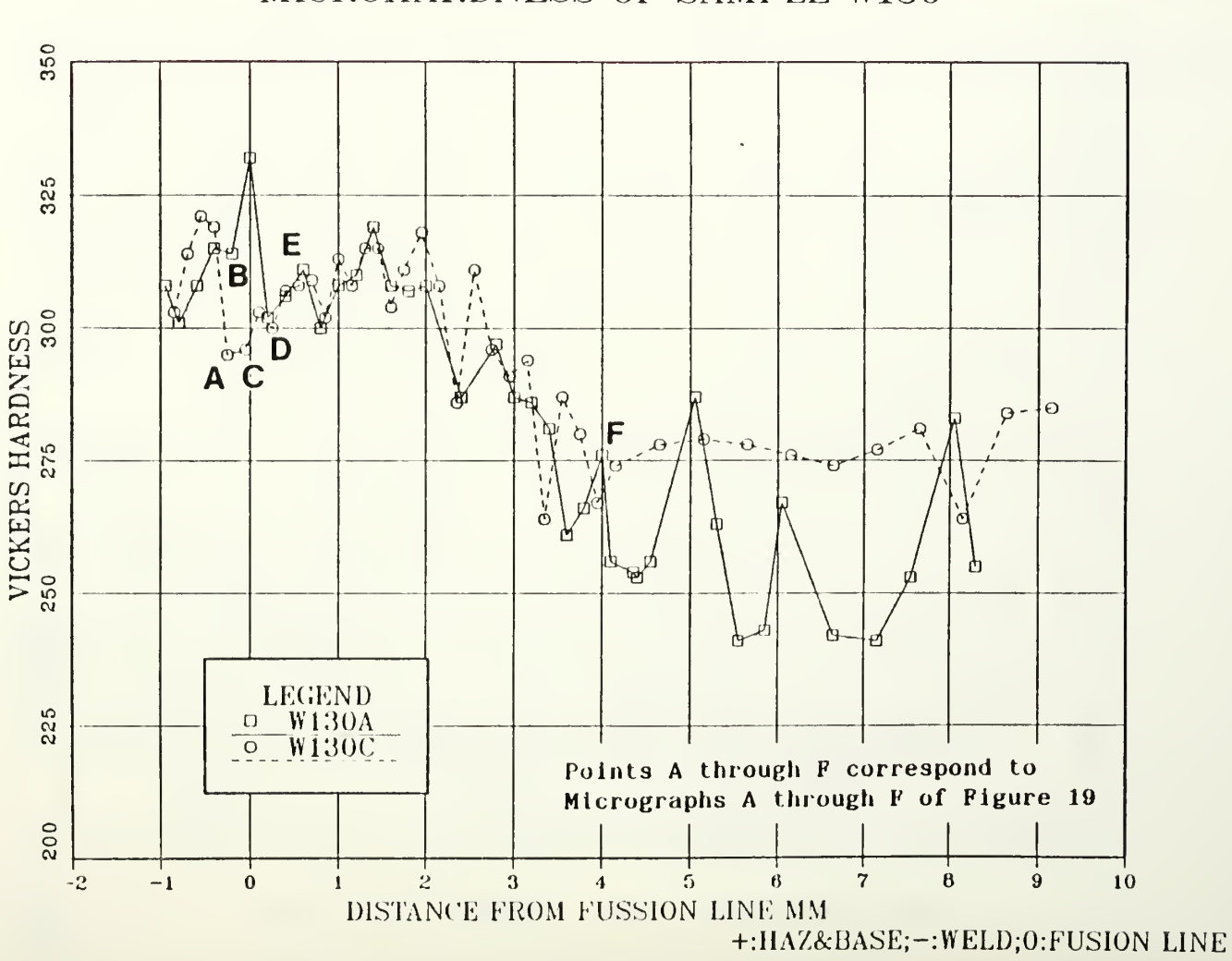

Figure 9. Microhardness Profile of W-130

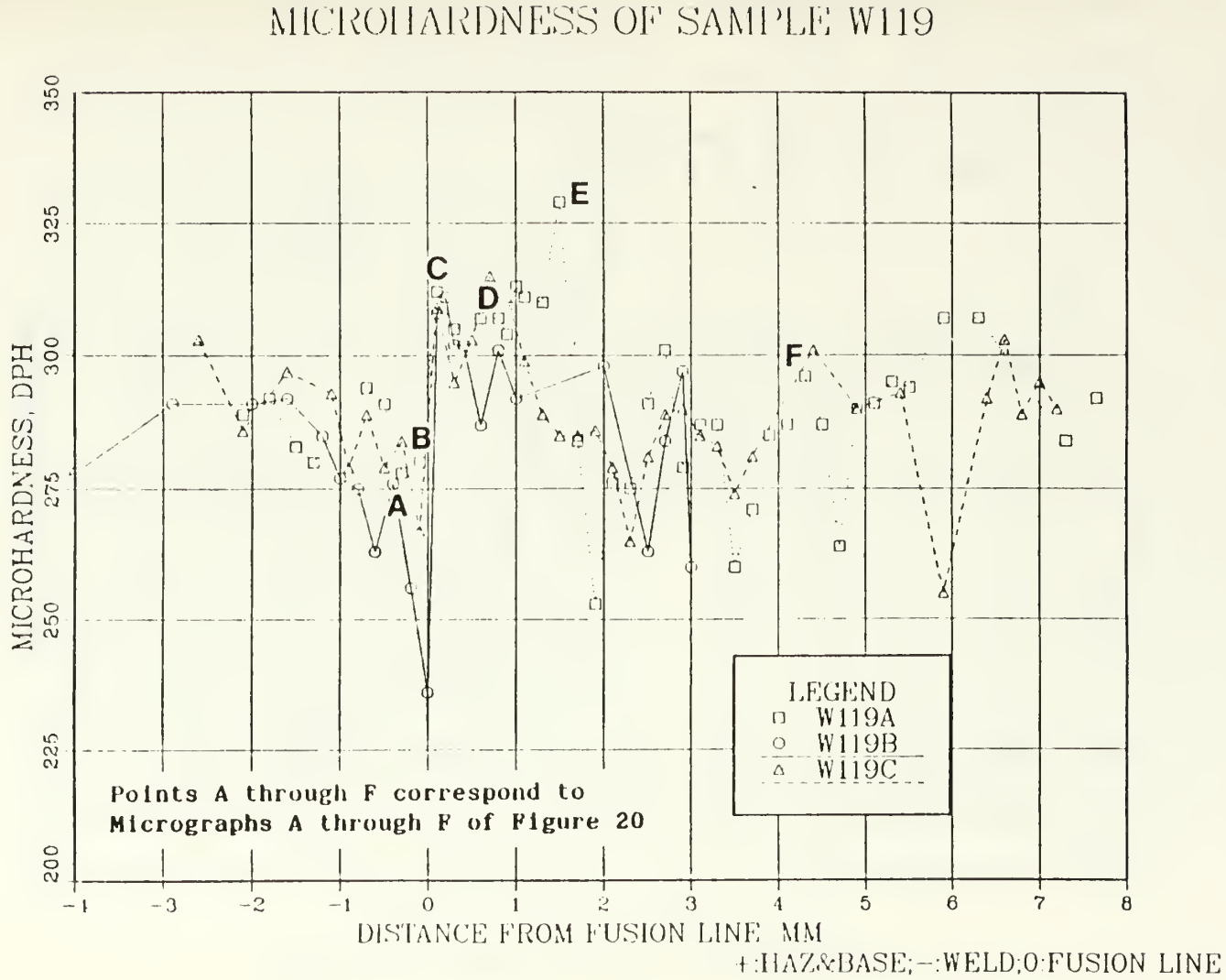

Figure 10. Microhardness Profile of W-119

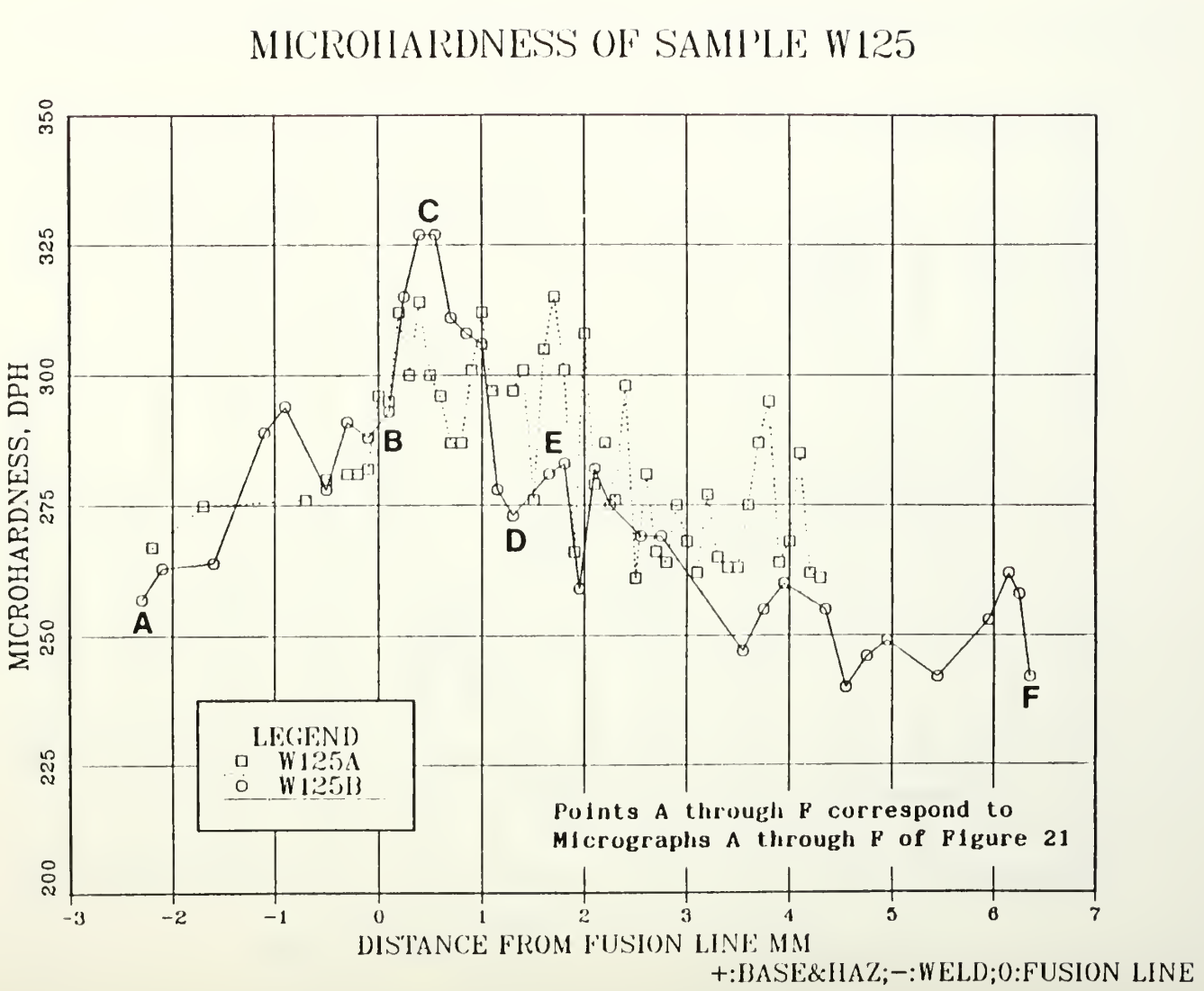

Figure 11. Microhardness Profile of W-125

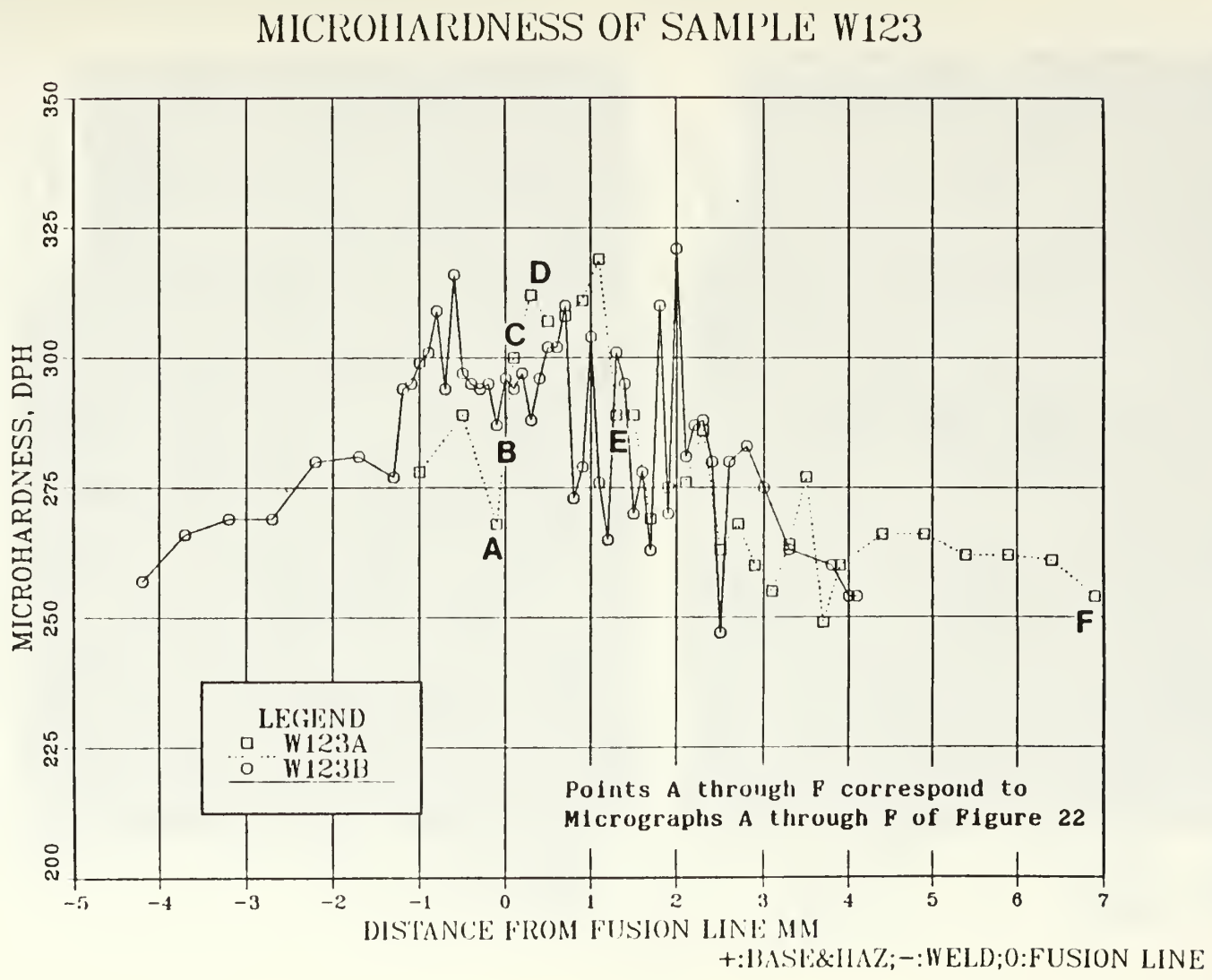

Figure 12. Microhardness Profile of W-123

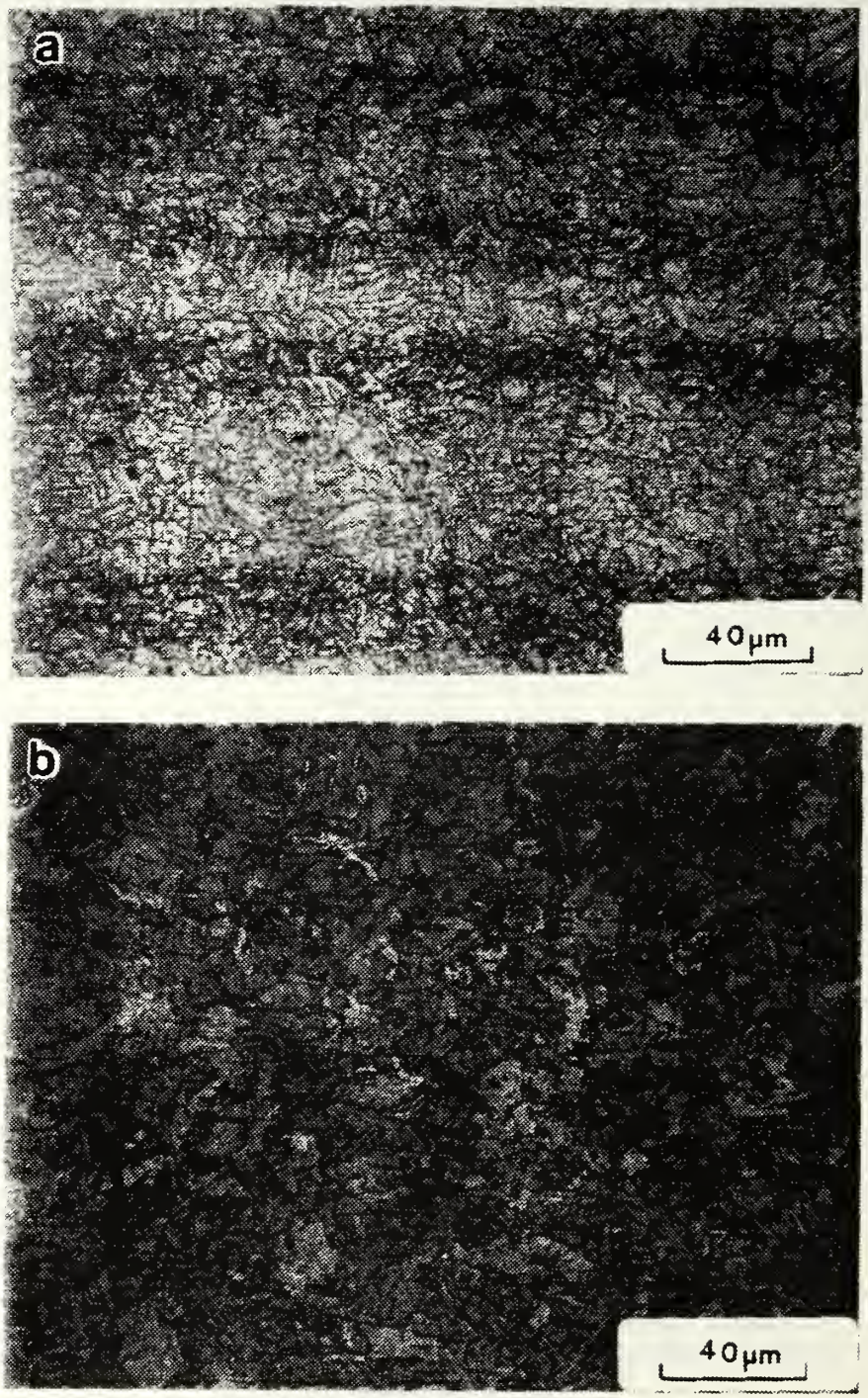

Figure 13. Optical Micrograph of Typical Bainitic Structure of Base Metal
a. 6.35 mm (1/4 inch) plate b. 19 mm (3/4 inch) plate

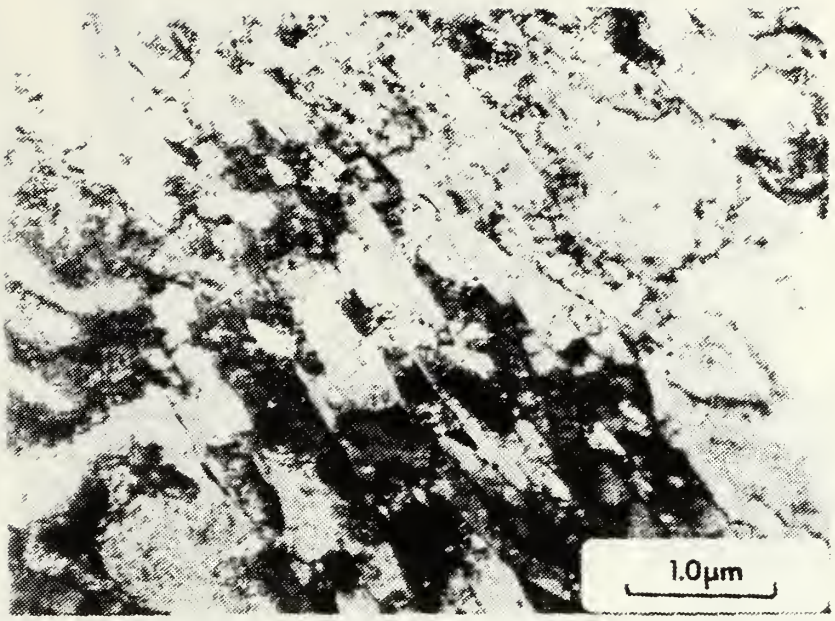

Figure 14. TEM Micrograph of 6.35 mm (1/4 inch) Base Metal

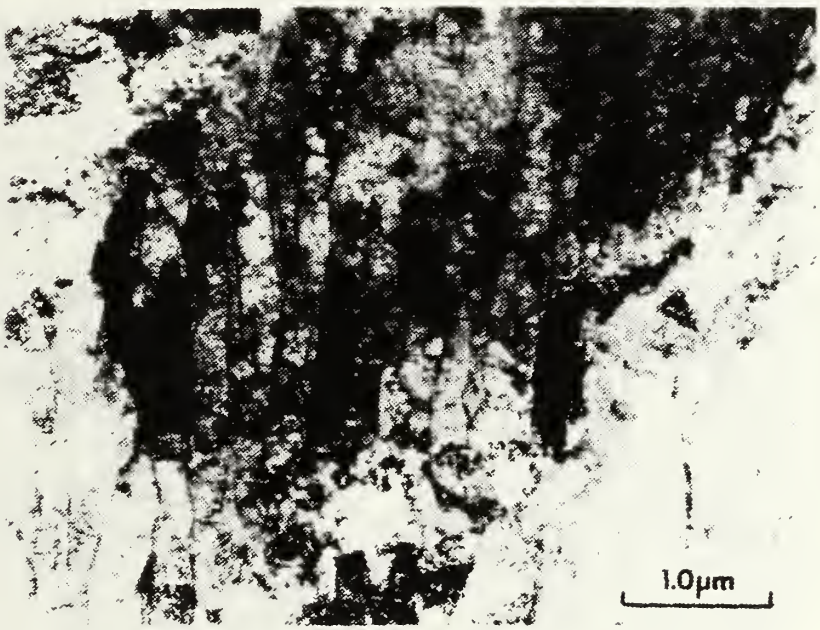

Figure 15. TEM Micrograph of 19 mm (3/4 inch) Base Metal

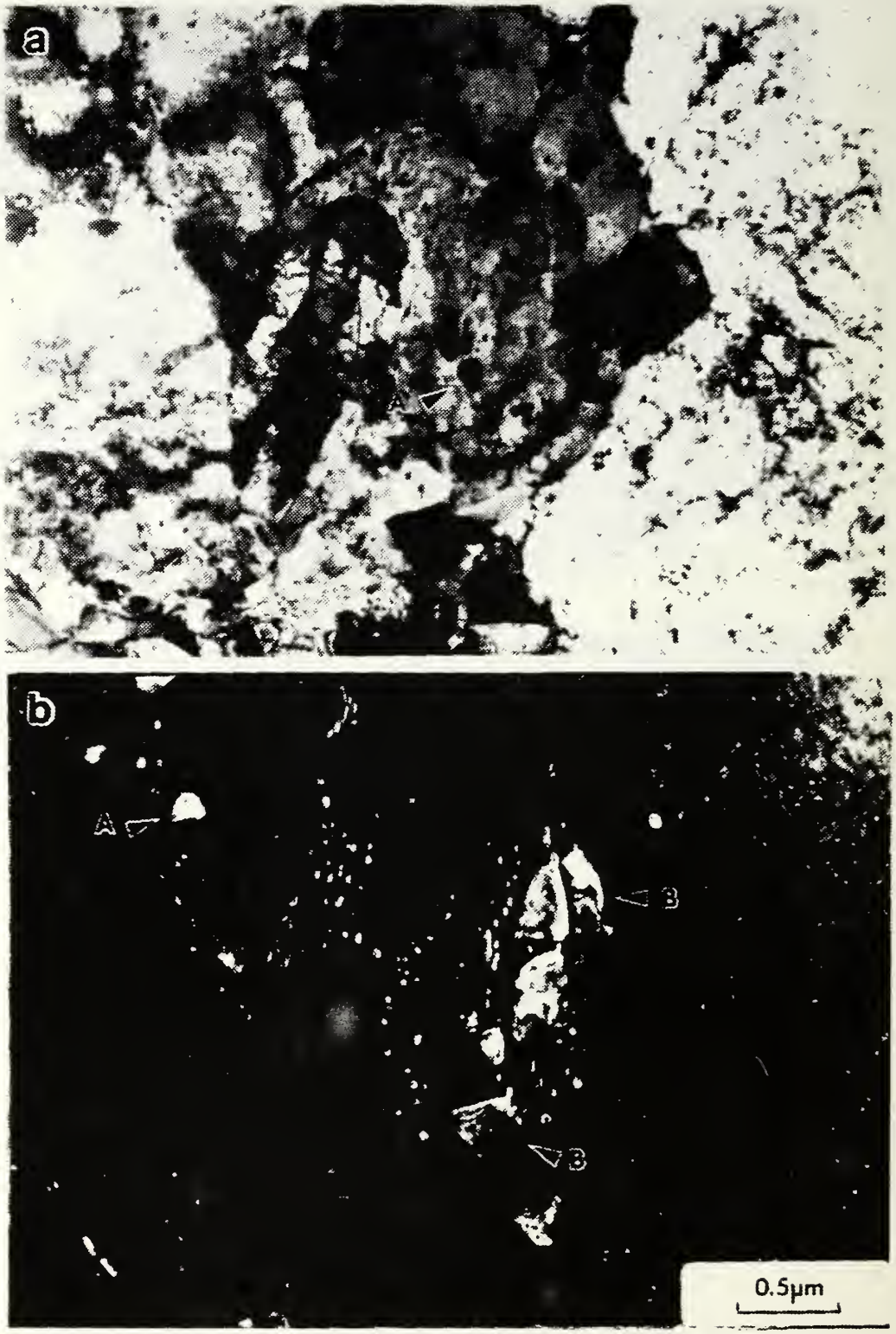

Figure 16. TEM Micrograph of 6.35 mm (1/4 inch) Base Metal
a. Bright Field b. Dark Field

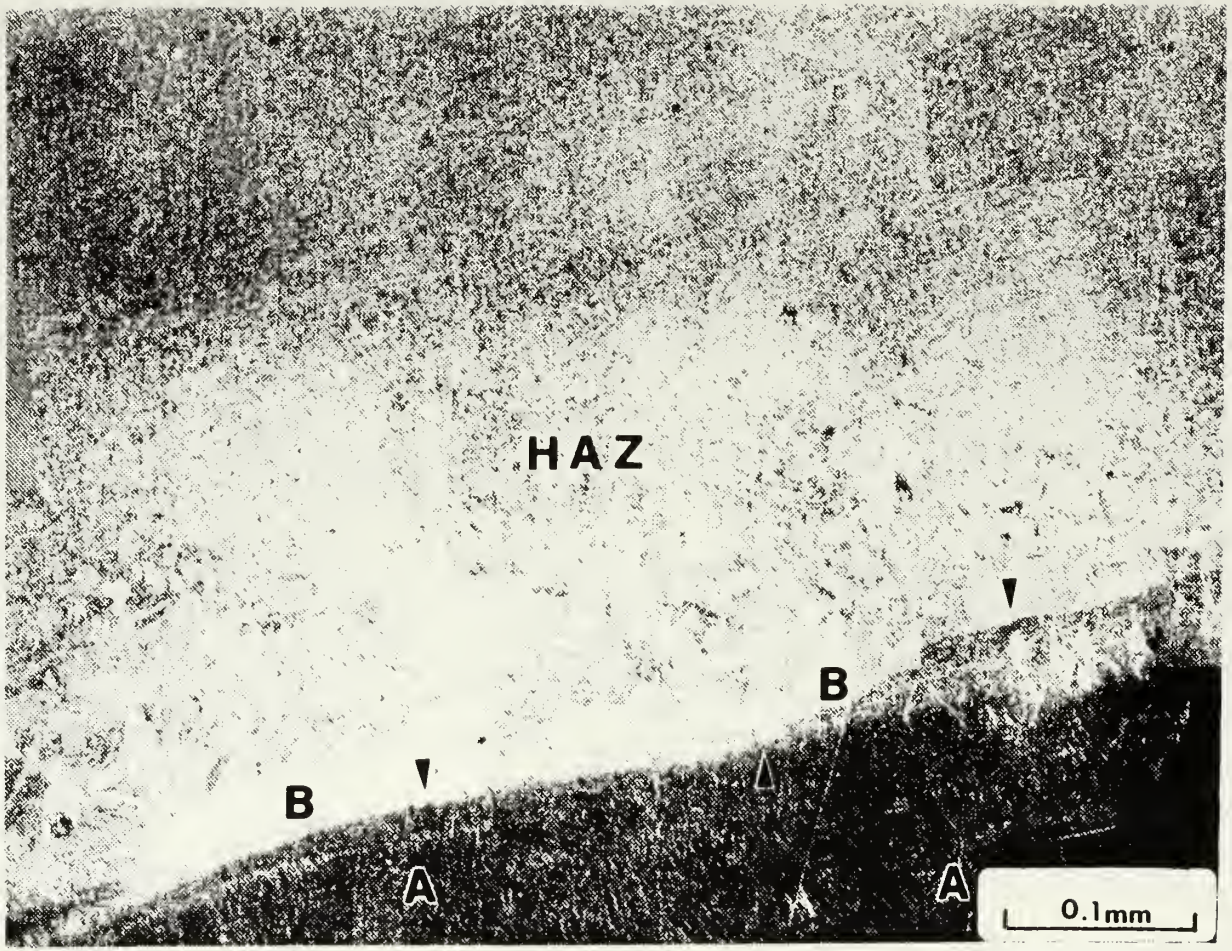

Figure 17. Optical Micrograph of HAZ of W130

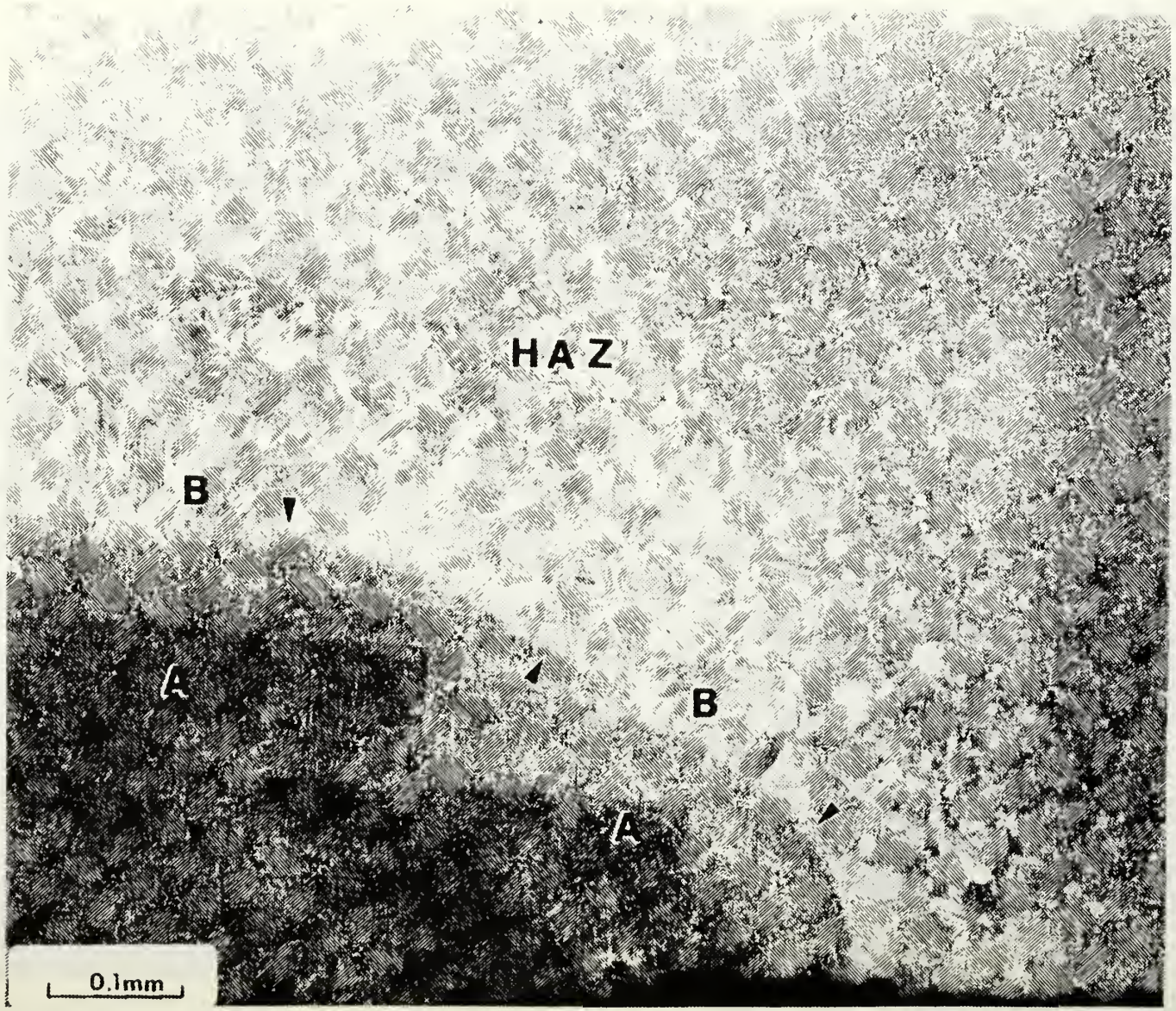

Figure 18. Optical Micrograph of HAZ of W119

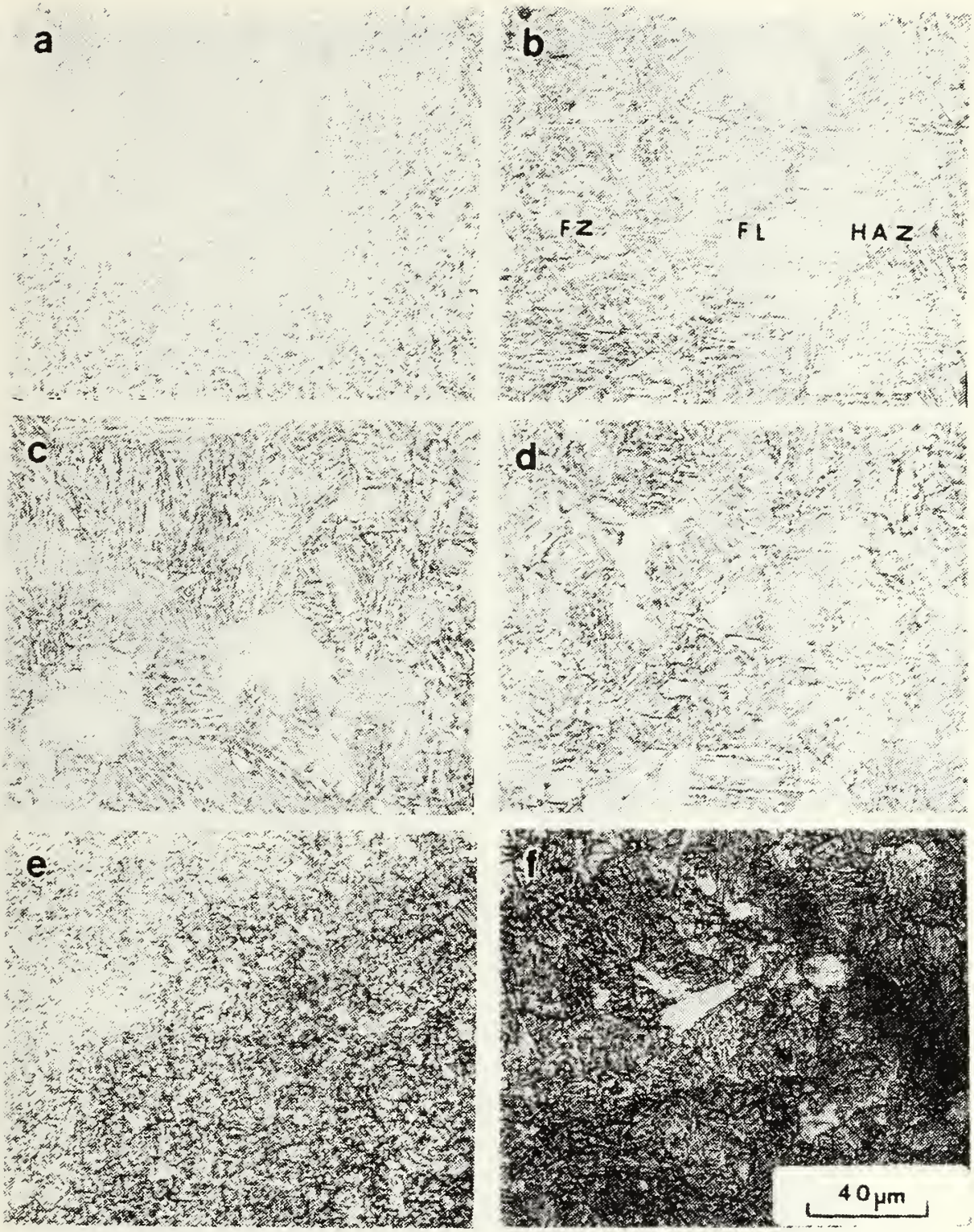

Figure 19. Optical Micrographs of W130
a. Fusion Zone b. Fusion Line c. Coarse HAZ
d. Coarse HAZ e. HAZ f. Base

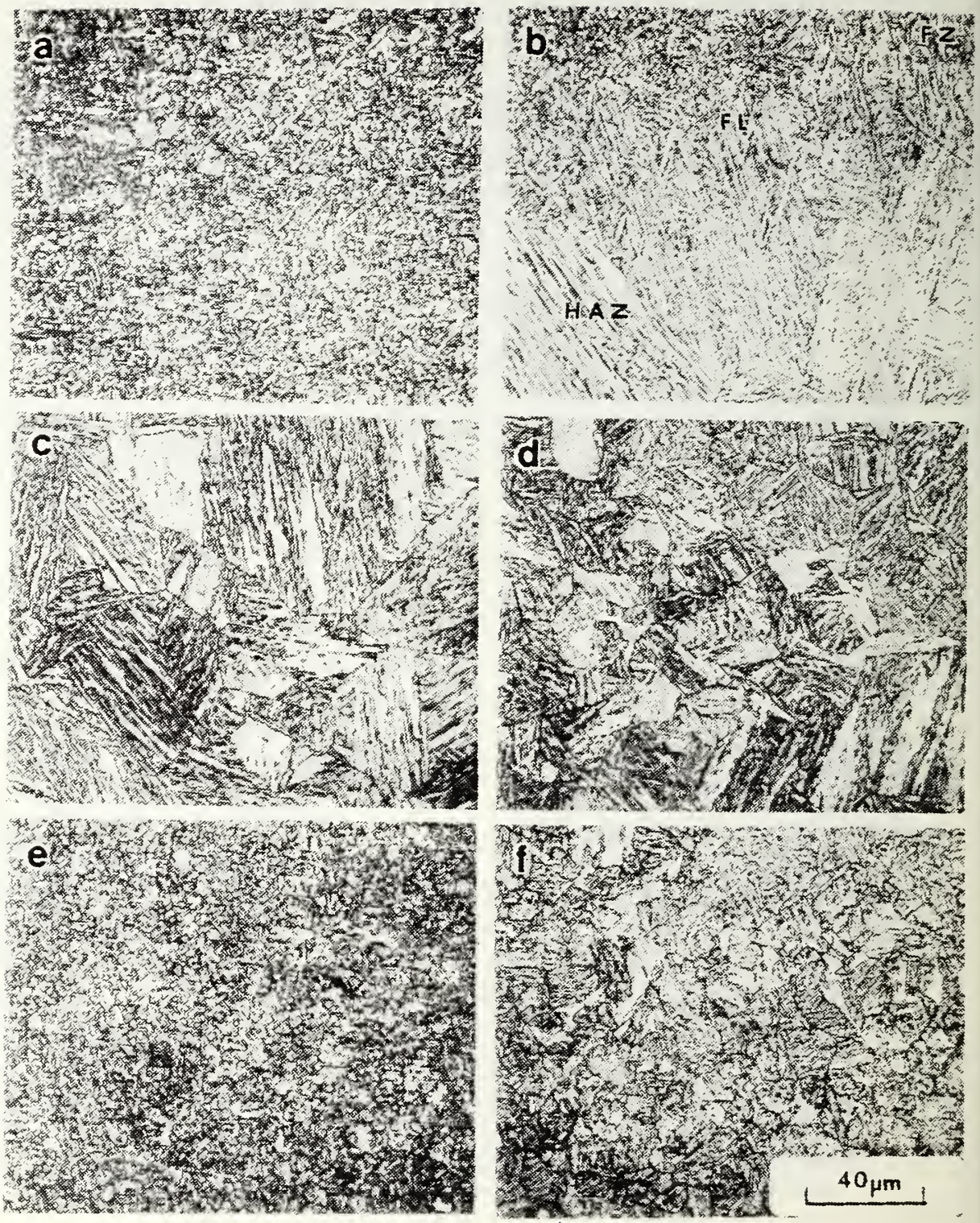

Figure 20. Optical Micrographs of W119
a. Fusion Zone b. Fusion Line c. Coarse HAZ
d. Coarse HAZ e. HAZ f. Base

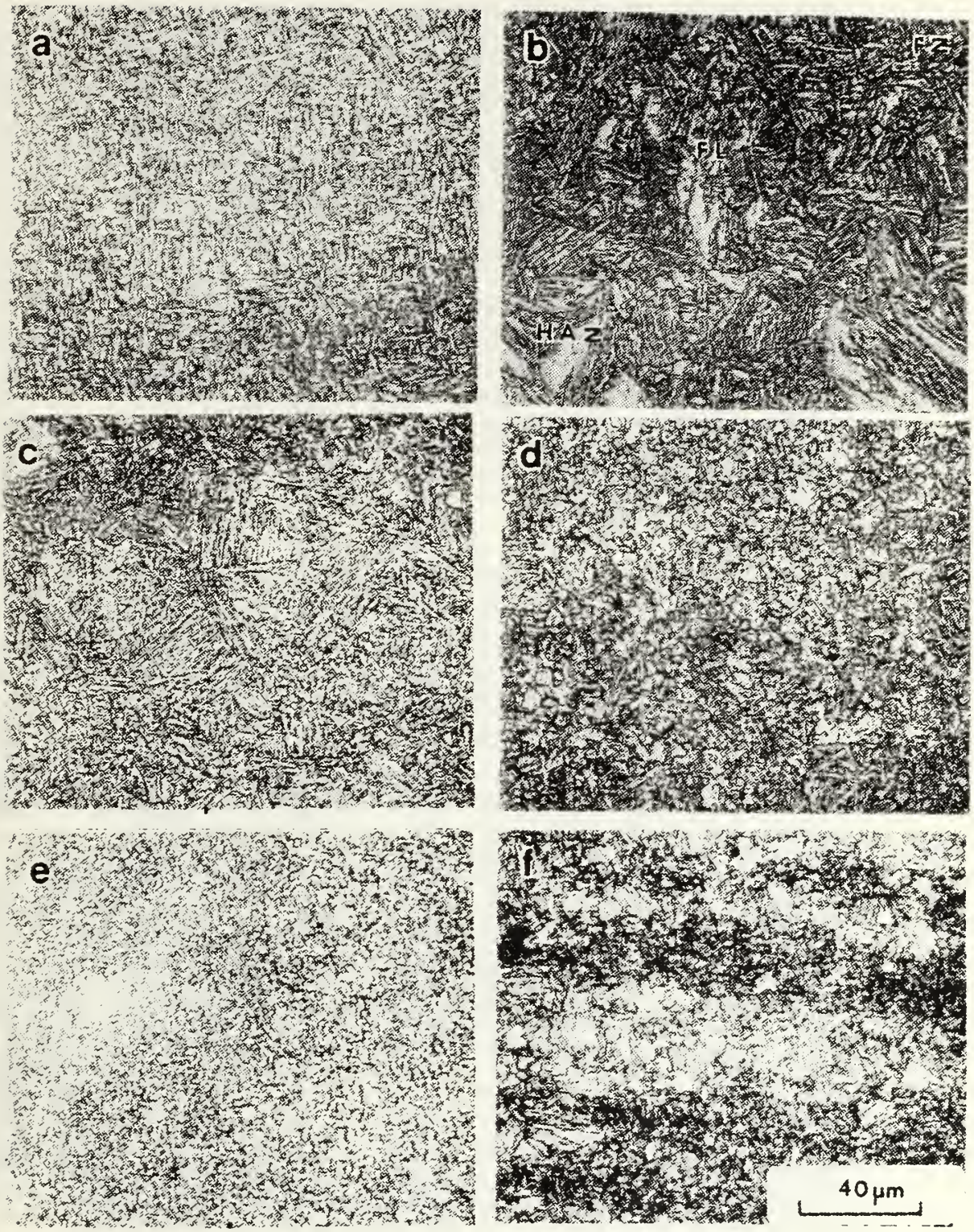

Figure 21. Optical Micrographs of W125
a. Fusion Zone b. Fusion Line c. Coarse HAZ
d. Coarse HAZ e. HAZ f. Base

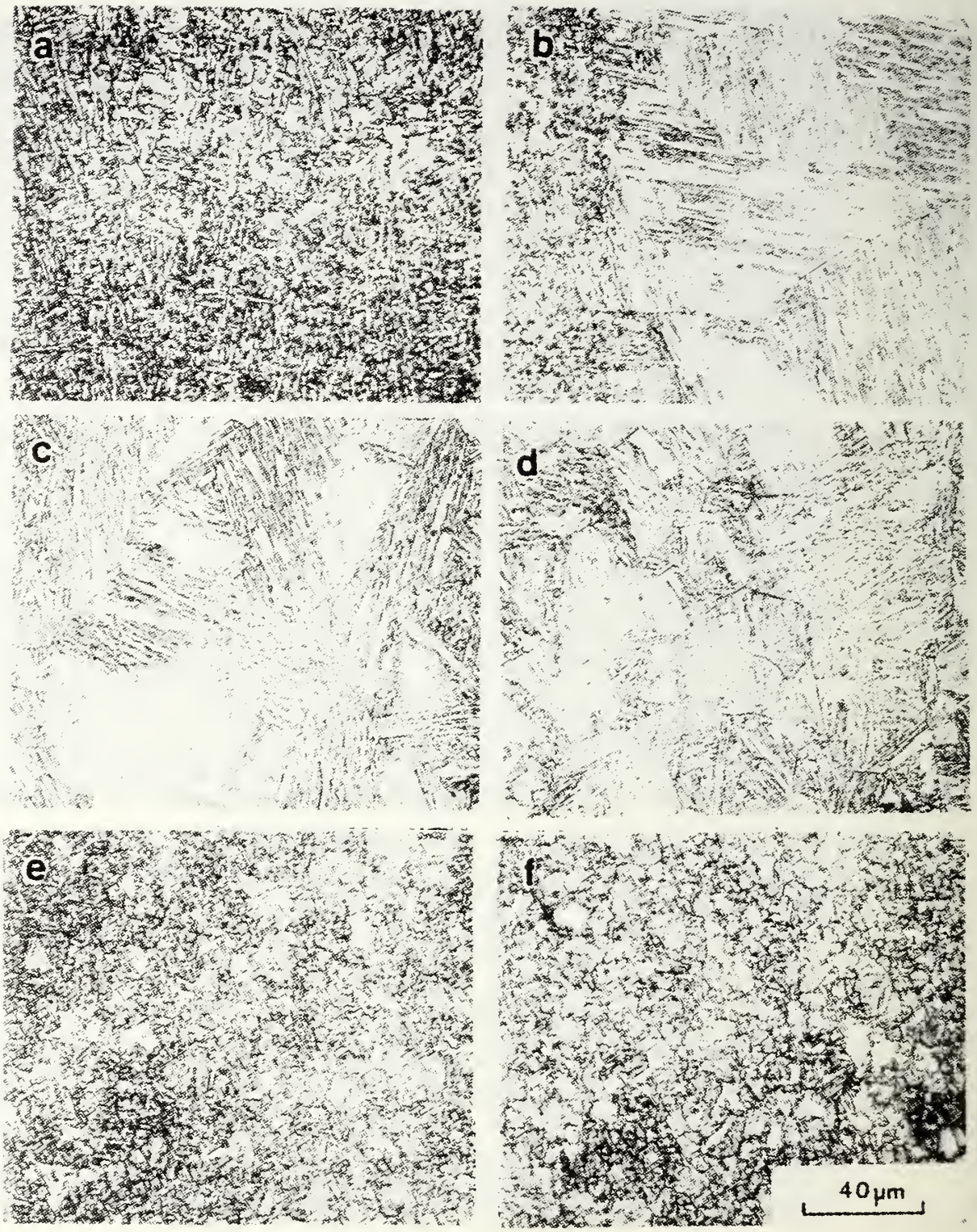

Figure 22. Optical Micrographs of W123
a. Fusion Zone b. Fusion Line c. Coarse HAZ
d. Coarse HAZ e. HAZ f. Base

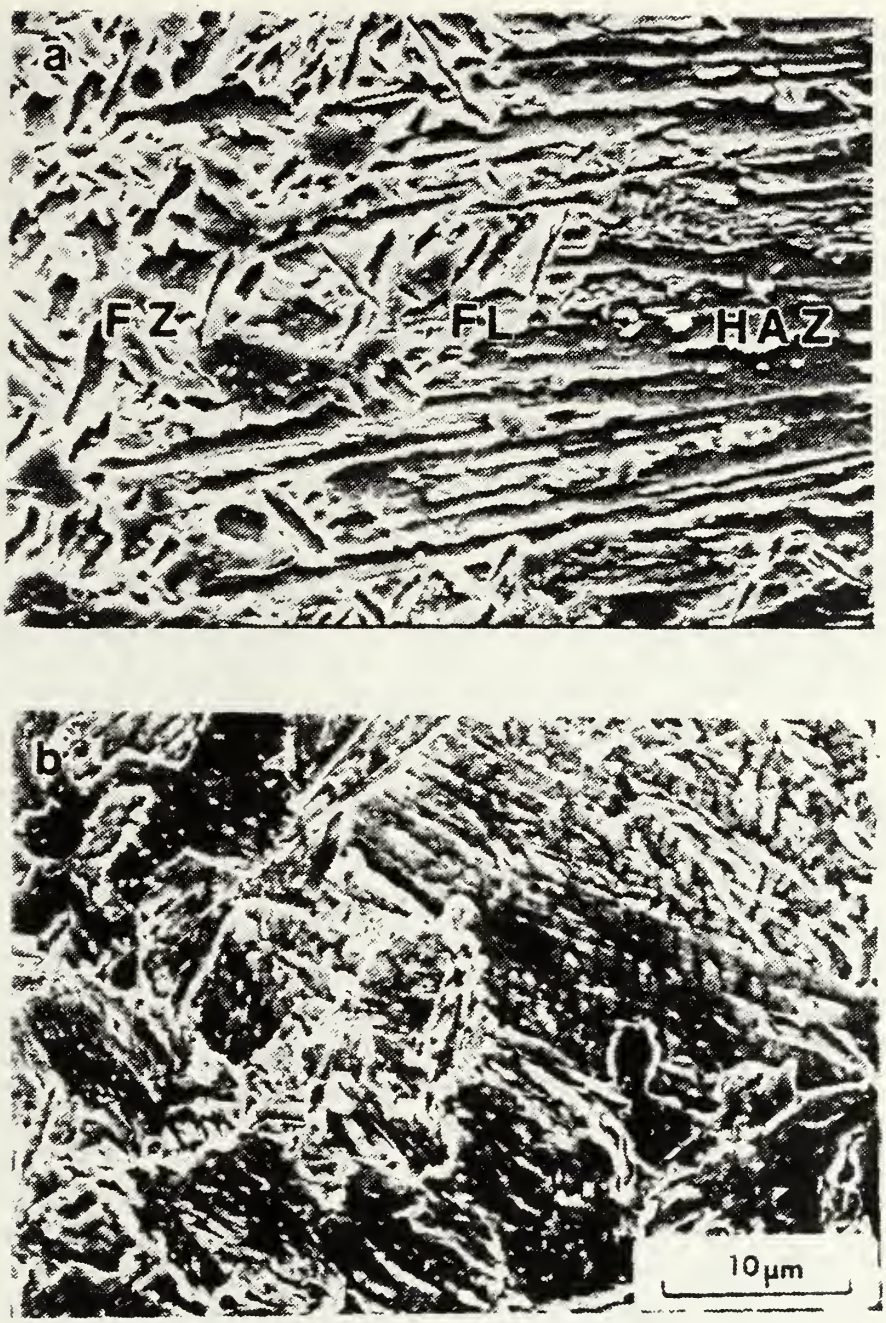

Figure 23. SEM Micrograph of W119
a. Fusion Line b. HAZ Adjacent to Base Metal

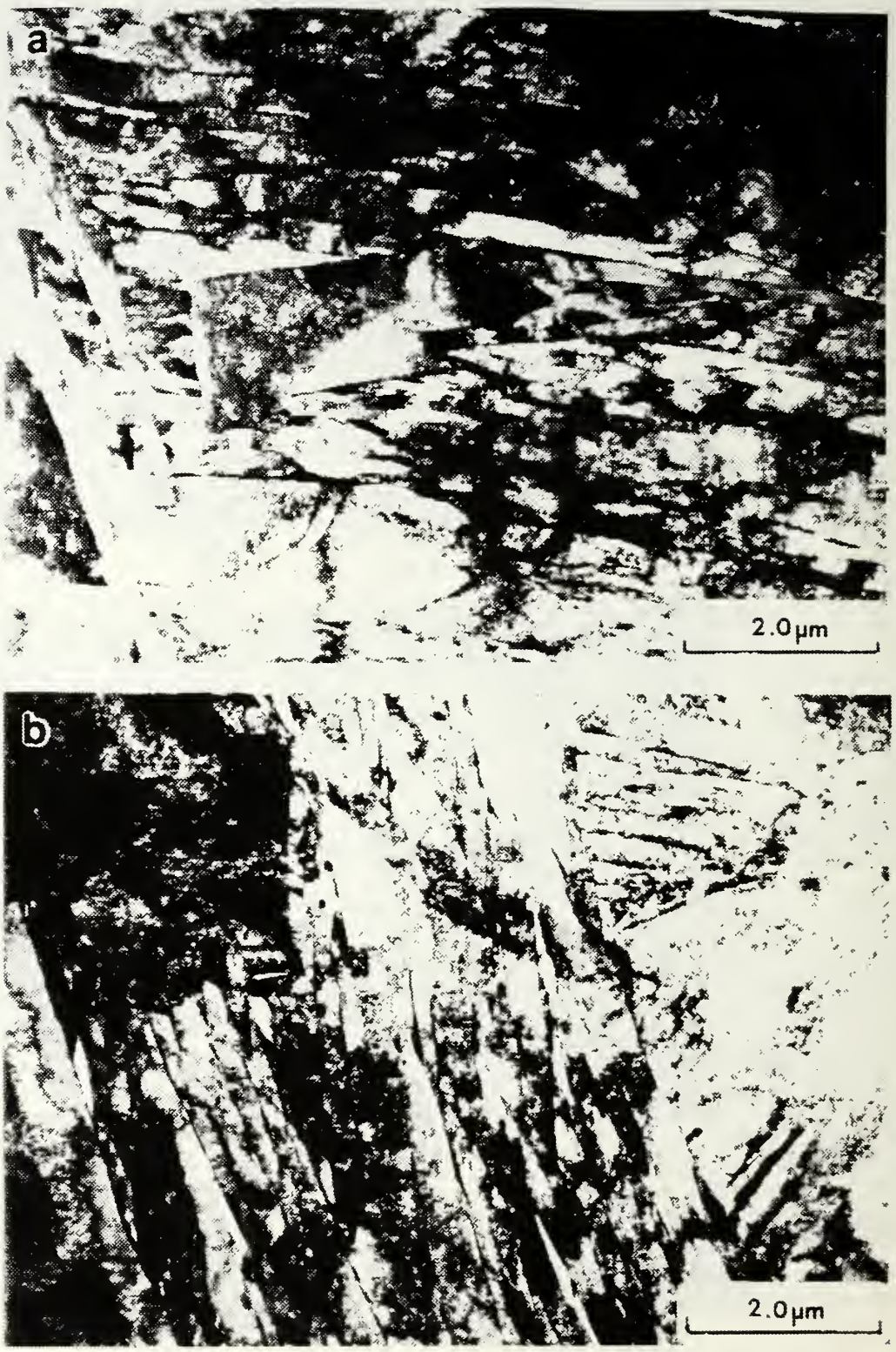

Figure 24. TEM Micrographs of Course Grain HAZ-W130
a. Lath Structure with High Dislocation Density
b. Lath Structure with High Dislocation Density

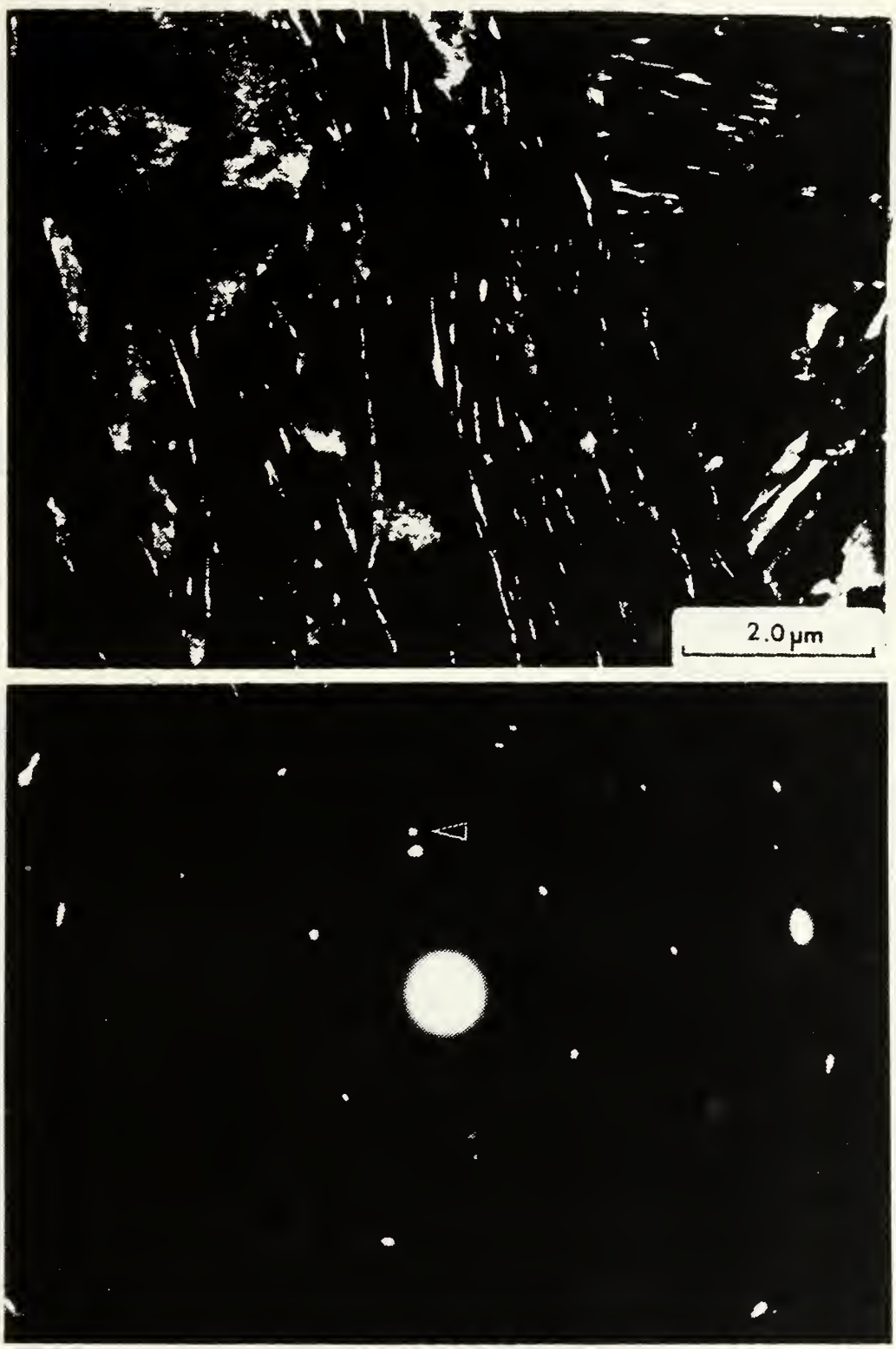

Figure 25. TEM Micrographs of Coarse Grain HAZ W130
a. Dark Field of Figure 22b Illustrating Interlath Distribution of Retained Austenite
b. Selected Area Diffraction, (002)γ Reflection Arrowed, Adjacent Reflection is (110)α

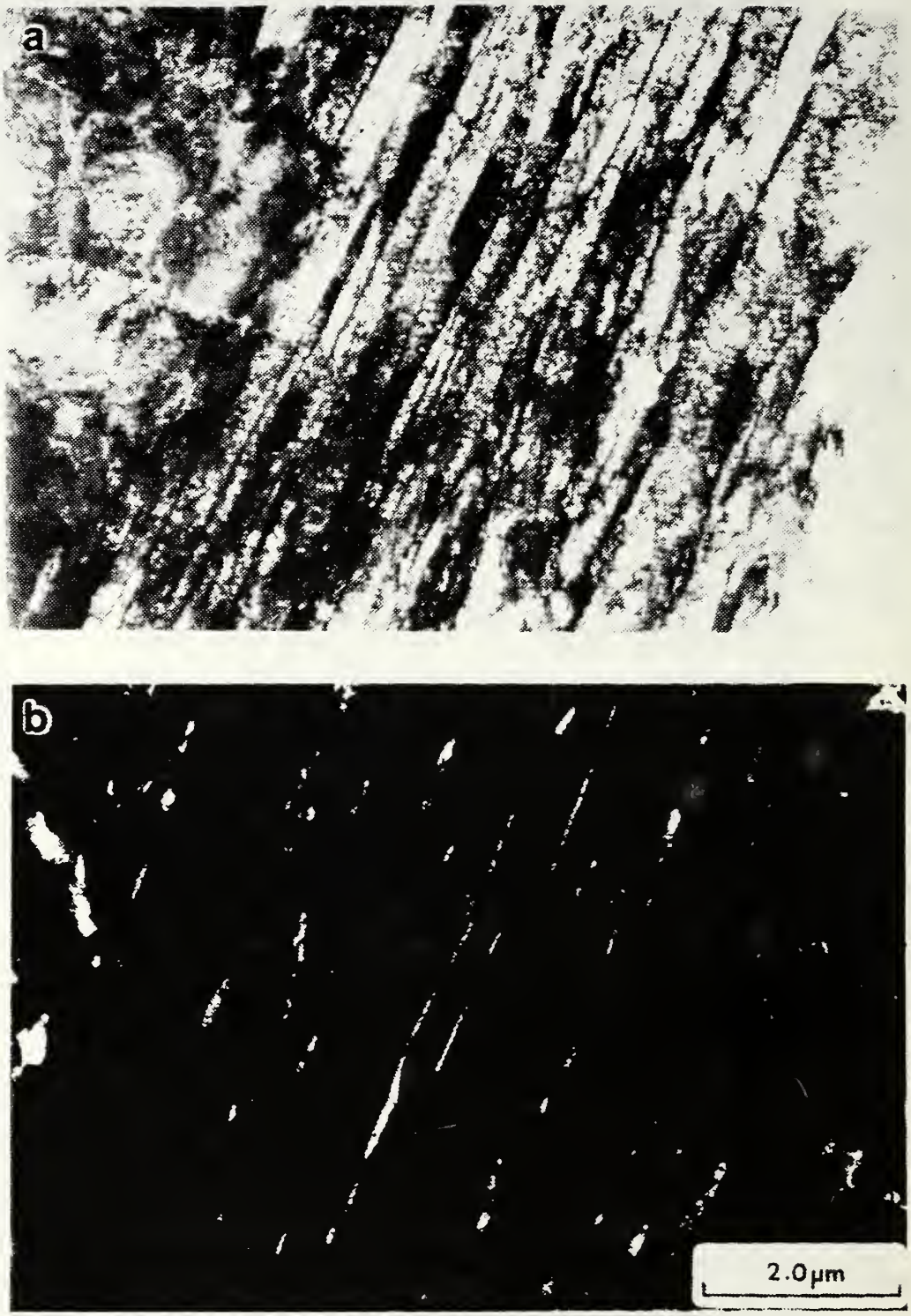

Figure 26. TEM Micrograph of Coarse Grain HAZ W119
a. Bright Field - Lath Structure
b. Dark Field - Taken with (002)γ Reflection

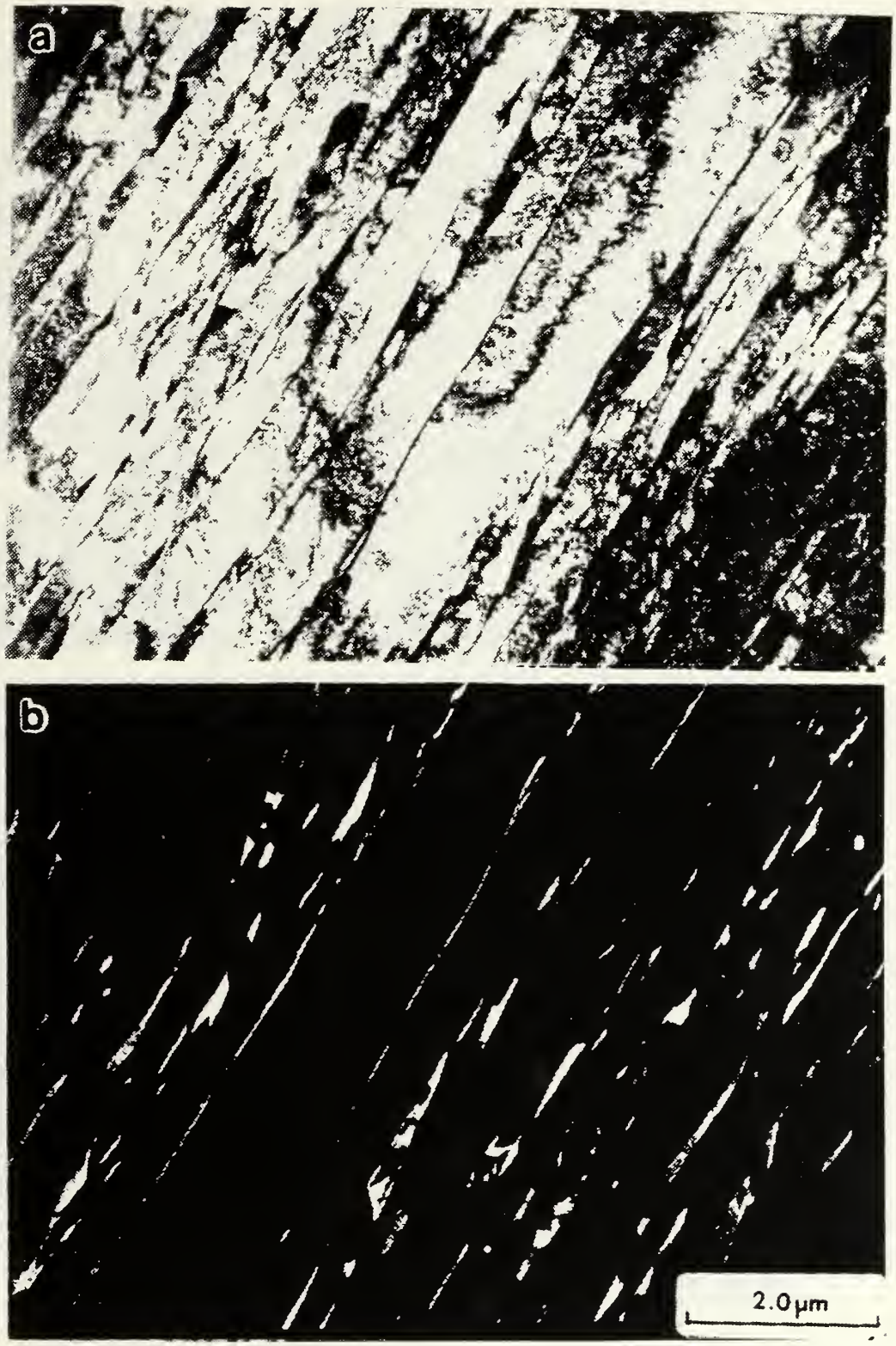

Figure 27. TEM Micrograph of Coarse Grain HAZ of W125
a. Bright Field b. Dark Field using γ Reflection

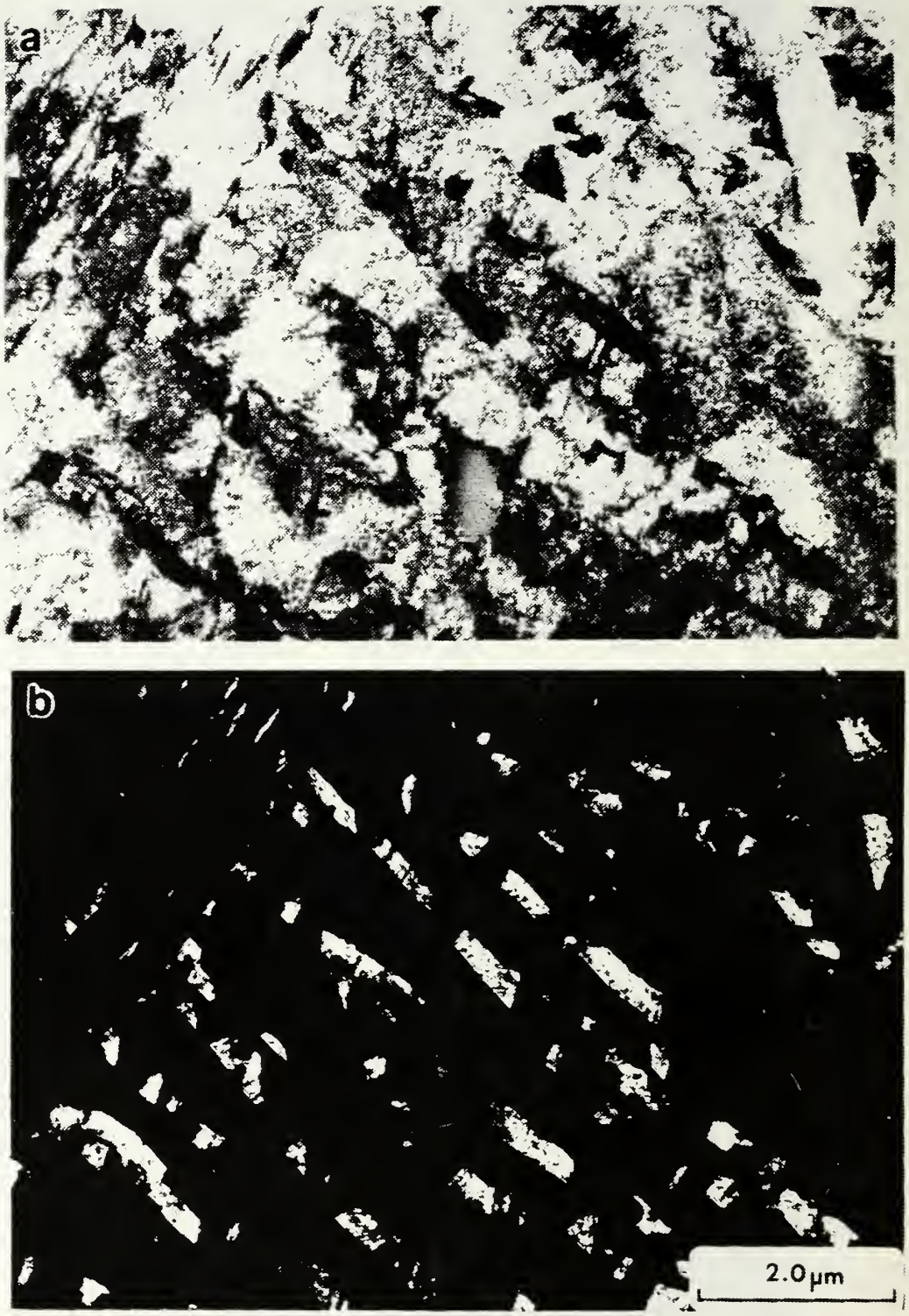

Figure 28. TEM Micrographs of Coarse Grain HAZ W125 with Retained Austenite a. Bright Field b. Dark Field using γ reflection

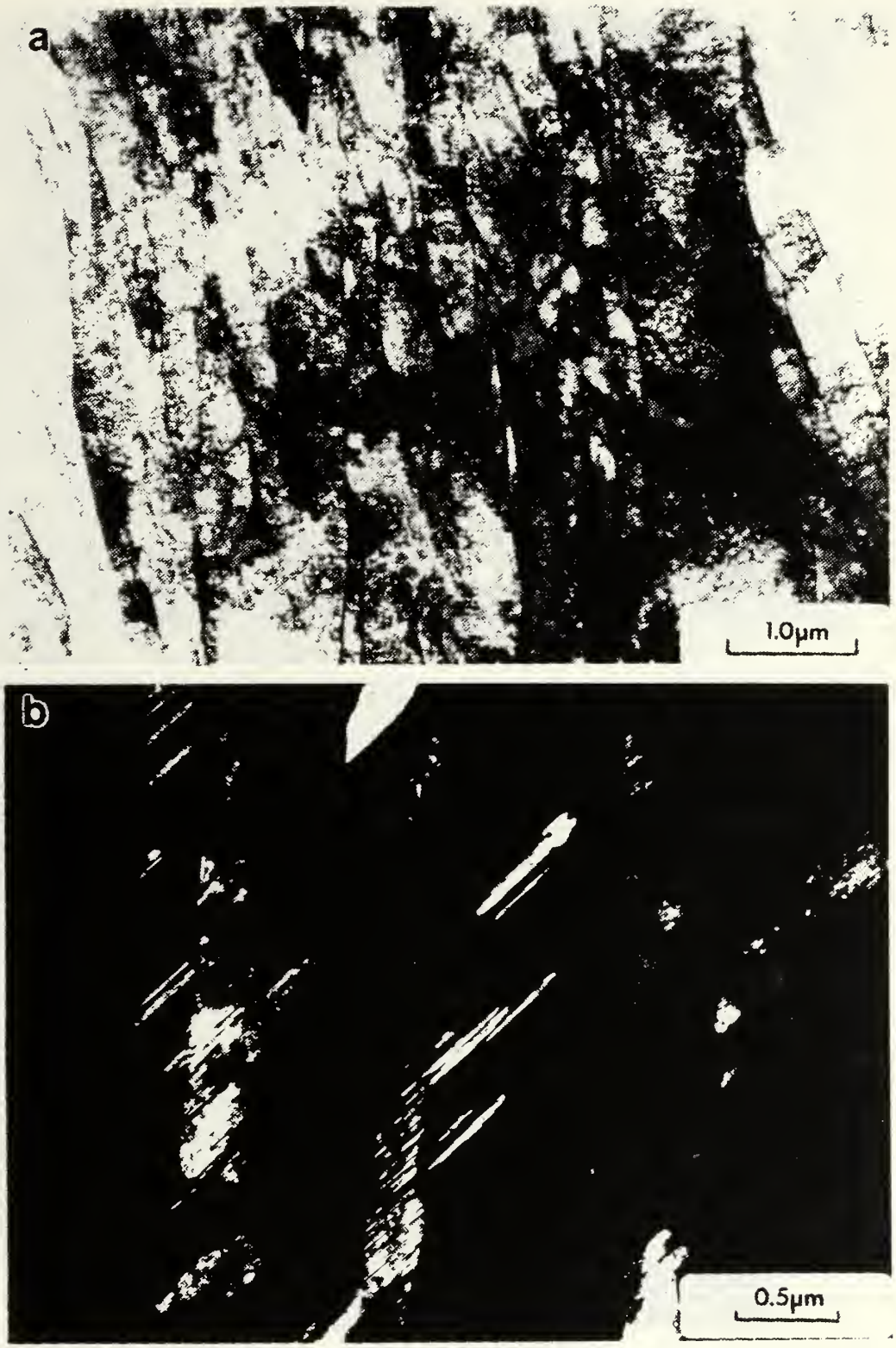

Figure 29. TEM Micrographs of Coarse Grain HAZ of W123
a. Bright Field b. Dark Field Showing Micro-twins

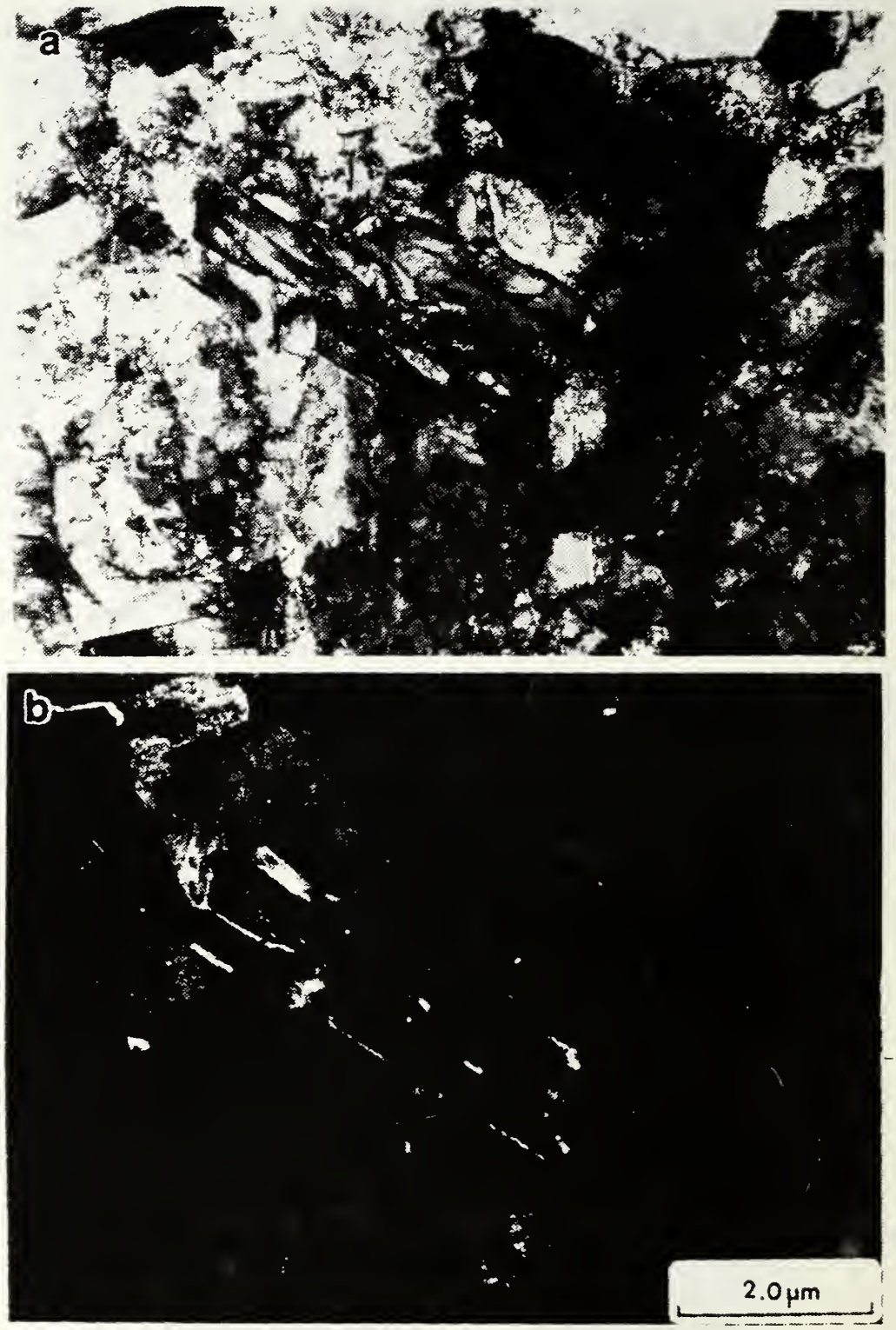

Figure 30. TEM Micrographs of W130
a. Bright Field b. Dark Field
using an ϵ-copper Reflection

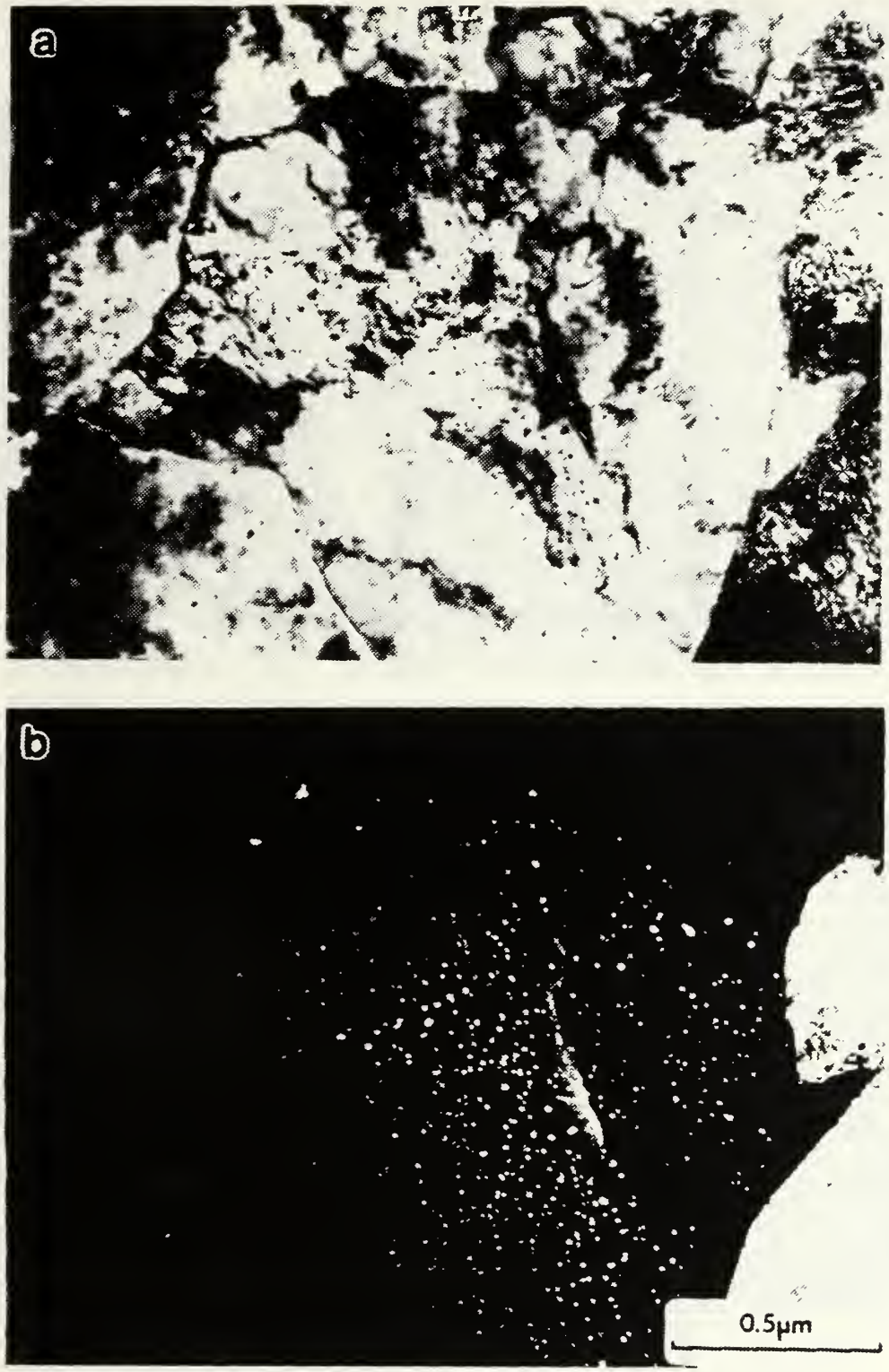

Figure 31. TEM Micrograph of W119
a. Bright Field - Coarse Copper Precipitates
b. Dark Field - Coarse Copper Precipitates

Figure 32. TEM Micrograph of Retained Austenite Particles in W119
a. Dark Field b. Dark Field

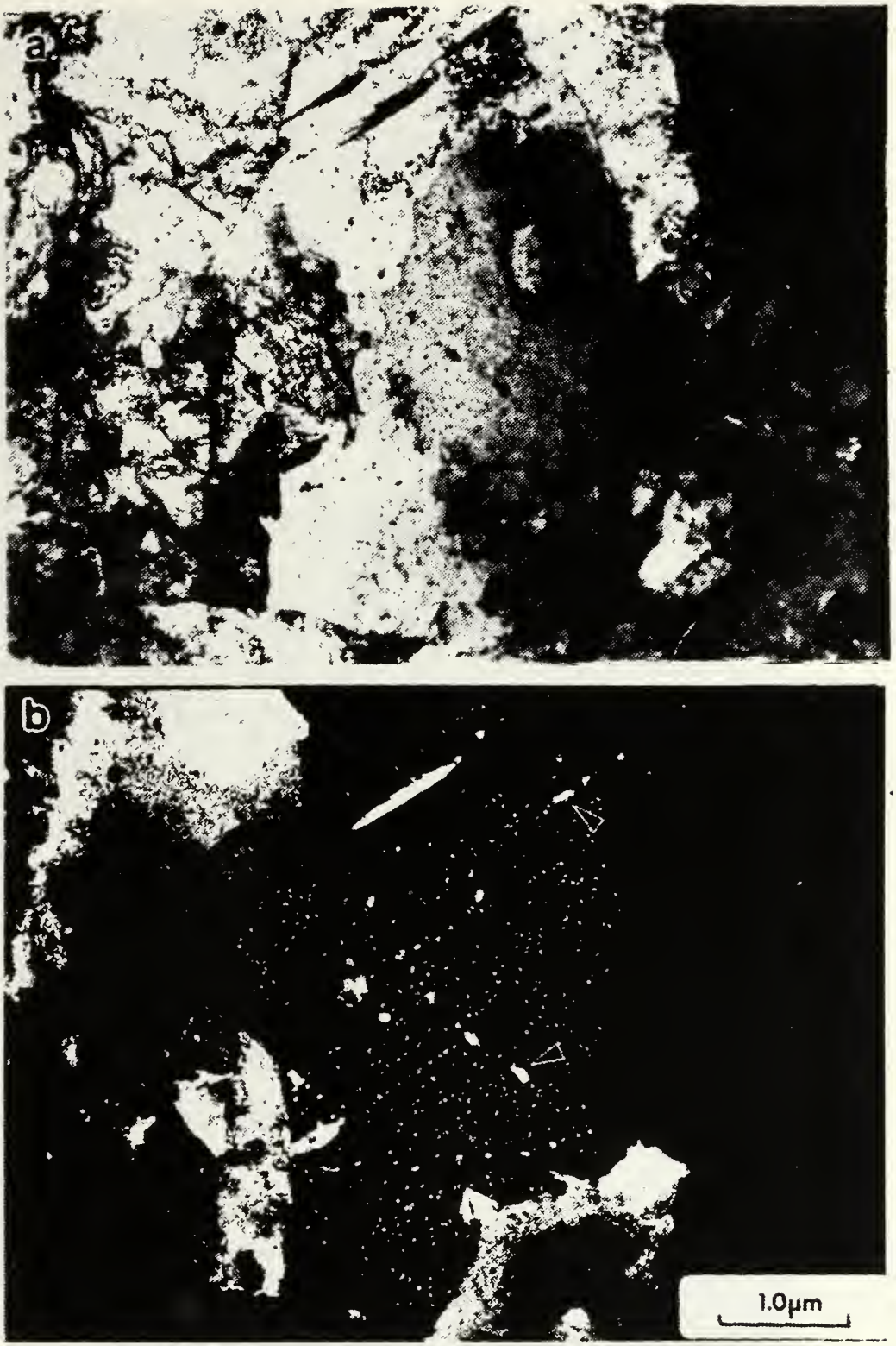

Figure 33. TEM Micrographs of W125
a. Bright Field b. Dark Field
using both an ϵ-copper and γ Reflection

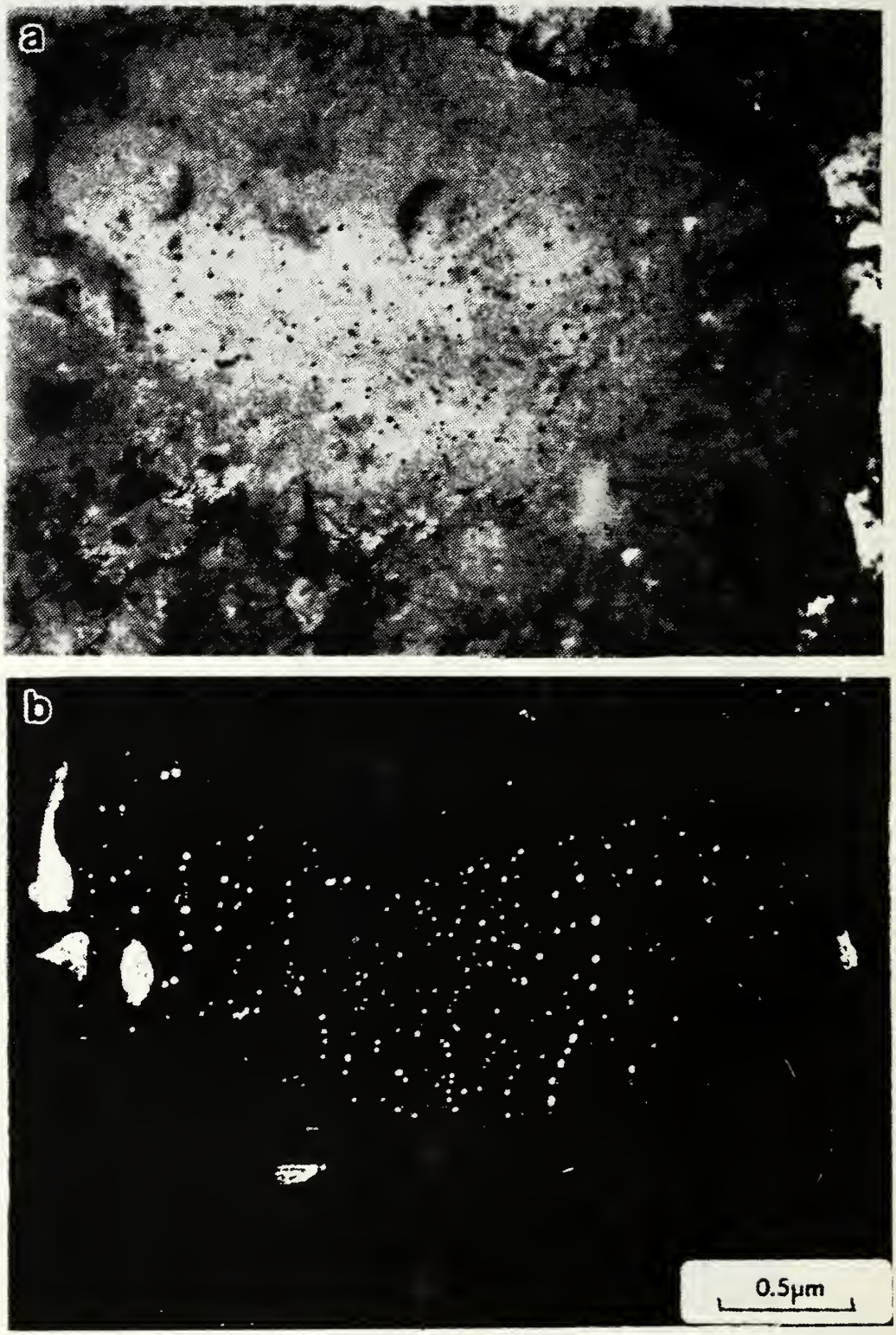

Figure 34. TEM Micrographs of W125
a. Bright Field b. Dark Field
using an ϵ-copper Reflection

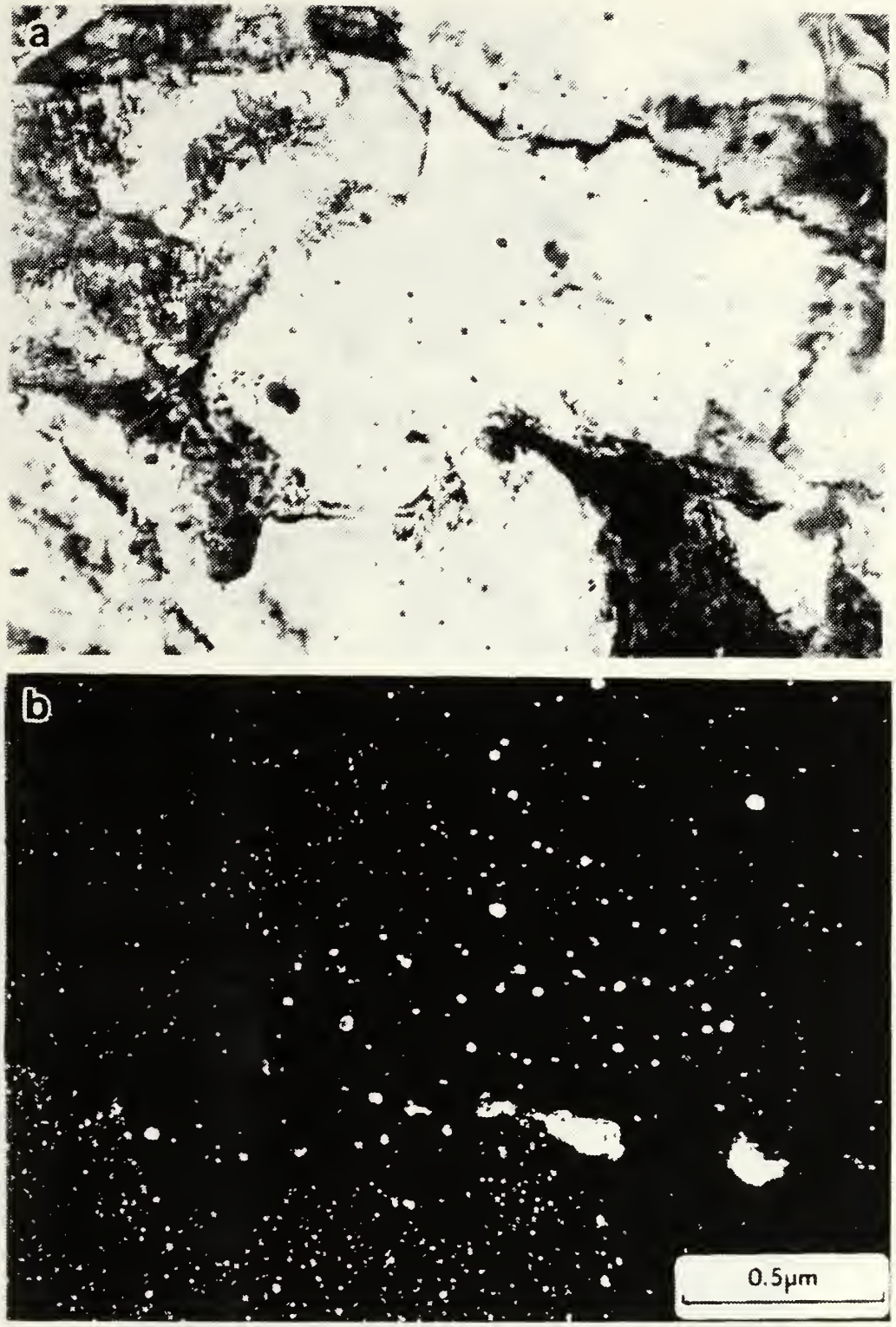

Figure 35. TEM Micrographs of W123
a. Bright Field b. Dark Field
using an ϵ-copper Reflection

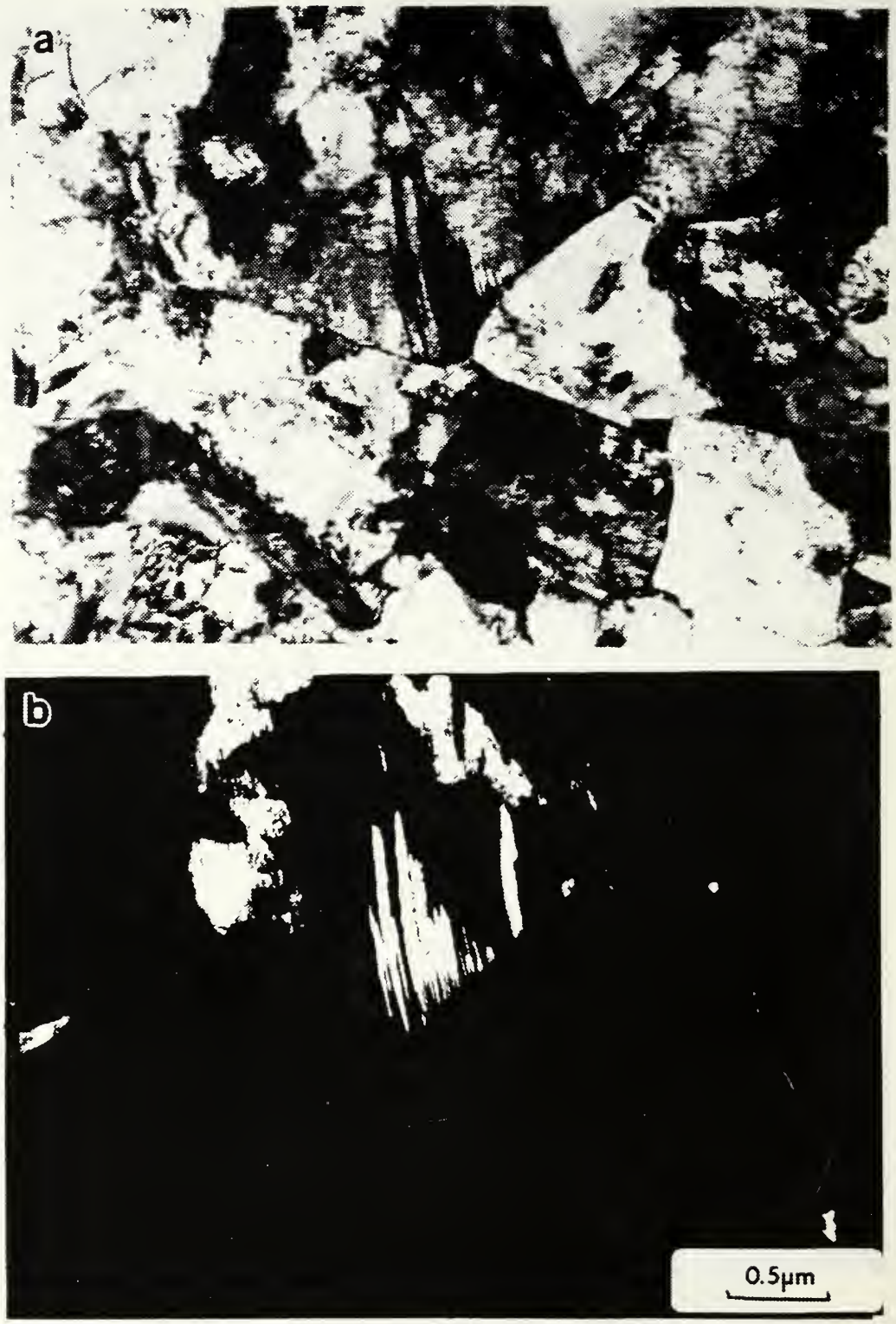

Figure 36. TEM Micrographs of W123 Polyganized Ferrite Grains with Microtwins
a. Bright Field b. Dark Field

LIST OF REFERENCES

1. Anderson, T. L., Hyatt, J. A. and West, J. C., "The Benefits of New High-Strength Low-Alloy (HSLA) Steels", Welding Journal, September 1987, p. 21.

2. Coldren, A. P. and Cox, T. B., "Development of 100 ksi Yield Strength HSLA Steel", DTNSRDC Report, SME-CR-07-86, July 1986, p. 2.

3. Metals Handbook, 8th Edition, Metallography Structures and Phase Diagrams. American Society of Metals, Vol. 8, Metals Park, Ohio, 1973, p. 4.50.

4. Miglin, M. T., Hirth, J. P., Rosenfeld, A. R. and Clark, A. T., "Microstructure of a Quenched and Tempered Cu-Bearing High Strength Low-Alloy Steel", Metallurgical Transactions A Vol 17A, May 1986, p. 791.

5. Coldren, A. P. and Cox T. B., p. 3.

6. Barret, C. R., Nix, W. D., Tetelman, A. S., The Principles of Engineering Materials, Prentice-Hall, Inc. 1973, p. 259.

7. Le May, I. and Krishnadev, M. R., "Fundamental Metallurgical Considerations", p. 23.

8. Le May, I., Schetky, L. McD., Krishnadev, M. R., "The Role of Copper in HSLA Steels, A Review and Update", Proceedings of AIME Conference, Wollongong, Australia, 20-24 August 1984, p. 64.

9. Metals Handbook Desk Edition, American Society for Metals, Metals Park, Ohio, 1985, p. 38.

10. Metals HandBook Desk Edition, p. 4.85.

11. Yano, S., Tanaka, K. and Aihara, S., "A 3.5% Nickel Steel for LPG Vessels", High Strength Low Alloy Steels, Proceedings of AIME International Conference, Wollongong, Australia, 20-24 August 1984, p. 297.

12. Xiuqiu, L. and Wenxuan, C., "The Effect of Manganese on the Recrystallization of Austenite in Low-Carbon Niobuim Steels", HSLA STEELS: Metallurgy and Applications, International Conference on HSLA Steels, Beijing, China 1985, p. 235.

13. Meyer, L., Stra Berger, C., Schneider, C., "Effect and Present Application of the Microalloying Elements N6, V, Ti,, Zr, and B in HSLA Steels", HSLA STEELS: Metallurgy and Applications , 1986, pp. 32-33.

14. Metals Handbook Desk Edition p. 4-61.

15. Le May, I. and Krishnadev, p. 29.

16. Lancaster, J. F., Metallurgy of Welding, 3rd Edition , George Allen and Unwin Ltd, London, 1980, p. 98.

17. Burna, R. F., "Effects of Preheat on Weldments of NICOP Steel." Master Thesis, Naval Postgraduate School, September 1983, p. 38.

18. Coldren and Cox, p. 13-14.

19. Miglin, M. T., et al, p. 798.

20. Goodman, S. R., Brenner, S. S. and Low, J. R., Jr., "FIM-Atom Probe Study of the Precipitation of Copper from Iron-1.4 At. Pct. Copper, Part I: Field-Ion Microscopy", Metallurgical Transactions, Vol. 4, October, 1973, p. 2363-69.

21. Wong, R. J., "Weld Process Development and Weldability of HSLA-100 Steel, Interin Report." TM-28-87-09, David Taylor Naval Research and Development Center, March 1987.

22. Mickelberry, K. D., "Microstructural Characterization of HSLA-100 GMW-Weldments", Master's Thesis, Naval Postgraduate School, September 1987.

23. Scoonover, T. M., Lukens, W. E., Pande, C. S., "Correlation of HAZ Microstructure with Peak Heating Temperature in HSLA-80 Steel Weldments", Unusual Techniques and New Applications of Metallography, Vol II, Proceedings of Metallography Symposium, ASM Metals Conference, 19-20 September 1984 and 14-15 October 1985 p. 97.

24. Miglin, M. T., et al, p. 798.

25. Honeycombe, R.W. K., Steels Microstructure and Properties, Edward Arnold Ltd, London 1981, p. 107.

26. Thomas, G., "Retained Austenite and Tempered Martensite Embrittlement", Metallurgical Transactions A. Vol. 9A, March 1978, pp. 442-447.

27. Easterling, K., Introduction to the Physical Metallurgy of Welding, Butterworths, London, 1983, p. 32.

28. Metals Handbook Desk Edition, p. 30-2.

29. Corderoy, D. J. H., "Welded Design in Q & T HSLA Steels", HSLA Steels, Proceedings of International AIME Conference, Wollongons, Australia, 20-24 August 1984, p. 128.

30. Ritchie, R. O., Cedeno, M. H. C., Zackay, V. F. and Parker, E. R., "Effects of Si Additions and Retained Austenite on SCC in Ultra High Strength Steels", Mettallurgical Transactions A. Vol. 9A Jan 1978, pp. 38-40.

31. Czyrca, E. J., Re: Technical Memorandum, 22 May 1986, Subj: HSLA-100 Steel Plate Receipt.

32. Kubaschewski, Ontrud, IRON-Binary Phase Diagrams, Springer-Verlag Berlin/Heidelberg, 1982.

BIBLIOGRAPHY

Bhadeshia, H. K. and Edmonds, D. V., Metallurgical Transactions, 10A, 1979, pp 895-907.

Chang, Y. A. et al., "Phase Diagrams and Thermodynamic Properties of Ternary Copper-Metal Systems". INCRA Monograph 17, INCRA, New York, 1979.

Huligren, R. and Desal, P.D., "Selected Thermodynamics Values and Phase Diagrams for Copper and Some of its Binary Alloys", INCRA Monograph 1, INCRA, New York, 1977.

Kubaschewski, Ontrud, IRON-Binary Phase Diagrams, Springer-Verlag Berlin/Heidelberg, 1982.

"Microstructural Characterization of Shielded Metal Arc Weldments of a Copper-bearing HSLA Steel", Materials Science and Technology, November 1985, Vol.1.

INITIAL DISTRIBUTION LIST

1.	Defense Technical Information Center Cameron Station Alexandria, VA 22304-6145	2
2.	Library, Code 0142 Naval Postgraduate School Monterey, CA 93943-5002	2
3.	Department Chairman, Code 69Hy Department of Mechanical Engineering Naval Postgraduate School Monterey, CA 93943-5000	1
4.	Associate Professor K. D. Challenger, Code 69Ch Department of Mechanical Engineering Naval Postgraduate School Monterey, CA 94943-5000	5
5.	Mr. R. J. Wong, Code 2821 David Taylor Naval Ship R & D Center Annapolis, MD 21402	2
6.	Mr. J. M. Losz, Code 69Lo Department of Mechanical Engineering Naval Postgraduate School Monterey, CA 93943-5000	1
7.	Lt. Kenneth D. Mickelberry, USN MPA Engineering Department USS Midway (CV-41) FPO San Francisco, CA 96601	1
8.	Lt. Gary P. Potkay, USN Class 4-87B Engineering Duty Officer School Mare Island Vallejo, CA 94592-5018	4
9.	Lcdr. W. Elger Code 05R NAVSEASYSCOM Washington, DC 20362-5101	1

18767 3

The
P74
c.1

Thesis
P748535 Potkay
c.1 Microstructural characterization of the heat affected zone of HSLA-100 steel GMA-weldment.

1 NOV 88
3 OCT 89
1 FEB 90
4 OCT 90

335988
32719
55755
35356

Thesis
P748535 Potkay
c.1 Microstructural characterization of the heat affected zone of HSLA-100 steel GMA-weldment.

Microstructural characterization of the

3 2768 000 79274 1
DUDLEY KNOX LIBRARY